Technical Report

The Second Research Dive on Image Mining for Disaster Management

January 2017

Advisor's Note

Initiating Collaboration to Enhance Indonesia's Disaster Management

When I received the invitation to serve as a research advisor for PLJ's research dive, I was very interested in the topic: image mining for disaster management. Wow! This topic is really cool and has many interesting challenges. Extracting information from a large number of images is one of my interests, and this event was my entry point to learn about its application in disaster management, collaborating with a wonderful research team. During the three days of the research dive, we learned together how image processing, data mining and remote sensing technologies can be used to extract useful information from image data obtained from social media to support disaster management. Many interesting ideas were proposed, discussed, implemented and evaluated from early morning to late at night in a very positive academic atmosphere. I really enjoyed learning many new things and working together with the wonderful teams: PLJ staff and scientists from universities and institutions across Indonesia. This is a good start for further collaboration in the future and I believe that we will be able to contribute significantly to disaster management in Indonesia.

Dr. Eng. Anto Satriyo Nugroho
Advisor for Image Processing

Anto Satriyo Nugroho is a computer scientist working for the Center for Information and Communication Technology, Agency for Assessment and Application of Technology, Republic of Indonesia. He received his B.Eng., M.Eng., and Dr.Eng. degrees in Electrical and Computer Engineering from Nagoya Institute of Technology of Japan, in 1995, 2000 and 2003 respectively. His research interests include Pattern Recognition & Image Processing with applied fields of interest in biometrics & computer aided diagnosis for malaria status identification from blood smears microphotograph. He joined the IT team of the General Elections Commission (KPU) during the Indonesian legislative election in 2009, and the Indonesian e-ID National Program "e-KTP" in 2012. In 2015, he served the Indonesian National Police as a researcher on scientific crime investigation related topics. Dr. Nugroho is a member of IEEE and vice president of the Indonesian Society for Soft Computing. He has received several awards, including a first prize award in the Meteorological Forecasting Contest 1999, conducted by the Neurocomputing Technical Group of The Institute of Electronics, Information and Communication Engineers, Japan, and the Satya Lencana Karya Satya in 2010 from the President of the Republic of Indonesia, for 20 years of devotion as a public official.

Nurturing Technology for Geo-related Problems

In disaster management activities, collaborative efforts are often under time pressure and available data can be complex and often conflicting. Access to and use of geospatial big data from satellite sensors and human sensors is necessary to help volunteers and decision-makers provide timely and better-coordinated disaster preparedness and response. The use of social media images for haze mitigation, pre- and post-volcanic eruption images for change detection and GIS modeling from drone imaging are all interesting topics. From the event we learned that the utilisation of techniques in visual analytics and image mining of geo-related data in disaster management is challenging but has potential benefits for society. The Research Dive initiative is an excellent breakthrough connecting technology and needs in humanitarian affairs. The cases and corresponding tasks during the event were perfect examples of many disaster aftermath scenarios, especially in Indonesia. Here, decisions must be made during a period when there is a lot of data (including big data) but it can often be conflicting. In many cases, it can go from bad to worse when there are no detailed maps and digital elevation models are unavailable. In some areas, there is no internet connection. Thus, the challenges that were given to the participants are valid.

I am excited to see how the groups accomplished the tasks in interesting ways. Further exploration on the topics of visual analytics and geospatial image analysis is needed to improve the quality of the results. In summary, the Research Dive event was a cool initiative. I was fortunate to meet great and enthusiastic colleagues and participants who are fully committed to finish their group task successfully. This event can be a good model to nurture today's technology to achieve the best solutions for our geo-related problems.

Trias Aditya K. M., ST, M.Sc, Ph.D
Advisor for Geographic Information System

Trias Aditya is Associate Professor in Geomatics Engineering at the Department of Geodetic Engineering, UGM. He received his MSc and PhD in Geo-informatics from ITC/Utrecht University on the topics of Geospatial Web Services for his MSc in 2003 and Atlas Metaphor for Geospatial Data Infrastructure for his doctoral study in 2007. He has published cartography and GIS related papers in journals and conferences as well as project reports on the topics of: participatory mapping, collaborative mapping, online cartography and cadastre.

Advisor’s Note

Finding Relevant Information to Support Disaster Mitigation

In my opinion, the event was great and very useful for disaster mitigation. Nowadays, we have entered an era where the internet is a powerful tool for accessing large amounts information. In order to get relevant, credible, and up-to-date information to support disaster mitigation, we need an effective sorting tool. I believe that the Research Dive could contribute to this aim, associated with the BNPB system, particularly to support the Data and Information team. In the past we have used drones to collect data on the condition of the land, but have not been able to effectively survey the area due to weather conditions. My team was looking for models of settlement damage and classification of damage zones from images, in order to better manage a disaster. Through the event I was also able to share current disaster management practice and the need to understand the risks and the near real-time impacts of haze, volcanic eruptions, floods and landslides. It is inevitable that the potential of real-time monitoring could support target programmes during implementation and improve decision-making processes.

Dr. Agus Wibowo
Domain Expert for Disaster Management

Dr. Agus Wibowo is the Head of the Information Division at the National Disaster Management Authority (BNPB) and is responsible for managing ICT infrastructure for Disaster Management. He was previously the Head of the Data Division where he was responsible for statistical and geospatial data collection, processing, modeling and visualization which aims to develop a statistical and geospatial database and information system for disaster management. Prior to joining BNPB, he worked at the Agency for the Assessment and Application of Technology as Remote Sensing and GIS researcher. He received his MSc from ITC Faculty of Geo-Information Science and Earth Observation, University of Twente and Wageningen Agricultural University in Enschede and Wageningen, the Netherland in 1997. In 2011, he obtained his doctorate in Geo-information, at the Faculty of Civil Engineering and Planning, Surabaya Institute of Technology, in Surabaya, Indonesia.

A Collaboration Platform Between Humanitarian Workers and Academia

When I first engaged in discussions on the Research Dive event “Image Mining for Disaster Management”, I had some mixed feelings. As a practitioner working in the humanitarian field for quite some time, my way of thinking and working is very practical and not as systematic as in research work. But during the preparations and discussions with the PLJ team, I must say that I was impressed and also appreciated the way they translated my practical way of thinking into something that very much can be included in research-based material.

I enjoyed the entire process, from the preparation to the actual event, and was so excited to see that the results turned out better than we expected. I would like to see more research and collaboration between humanitarian workers and educational practitioners and researchers. I hope to see follow-up actions and deeper research on the results.

Faizal Thamrin
Domain Expert for Disaster Management

Faizal Thamrin is the Information Management Officer at the UN-OCHA Indonesia office. He serves as the UN focal point for data and information coordination during emergency response. His office aims to better integrate humanitarian work with disaster recovery, sustainable development and cross-cutting issues as well as improve the speed and accuracy of information delivered, which creates a shared frame of reference that enables decision-makers to co-ordinate and plan response programming based on best available knowledge of humanitarian needs and a clear understanding of each organization’s capacity. Mr. Thamrin has been working in the information management field for over 10 years. He has responded to different major sudden onset emergencies such as the 2006 Java earthquake, 2009 Sumatra earthquake, 2010 Pakistan floods, 2013-14 Typhoon Haiyan and many small to medium-scale disasters in Indonesia.
Mr. Thamrin wishes to work together with passionate collaborative partners with their new ideas and innovation to help strengthen the humanitarian community in Indonesia.

Executive Summary

Indonesia is one of the most disaster-prone countries in the world. In recent years, both natural and manmade disasters, including haze from forest fires, volcanic eruptions, floods and landslides, have resulted in deaths, destruction of land areas, environmental impacts, and setbacks to the economy. Faced with these risks, the Government of Indonesia is continually challenged to improve its disaster management practices and post-crisis responsiveness.

Digital data sources and real-time analysis techniques have the potential to be an integral part of effective disaster management planning and implementation. Among these techniques, the use of image-based data can further enhance knowledge discovery related to this issue. When mined and analysed effectively, imagery data sourced from social media, satellite imagery, and Unmanned Aerial Vehicles (UAVs) can capture valuable ground-level visual insights. This data can be used to inform disaster-related decision-making and improve response efforts.

Using 5,400 images related to haze collected from social media, gigabytes of time-series satellite imagery capturing an active volcano pre- and post-eruption from the National Institute of Aeronautics and Space Indonesia (LAPAN) and Google Earth, as well as UAV images of the recent landslides in Garut, West Java, Pulse Lab Jakarta recently invited image mining and Geographic Information System (GIS) enthusiasts to dive into this data.

On 13 - 16 November 2016, Pulse Lab Jakarta organized a Research Dive on Image Mining for Disaster Management, hosting 16 researchers from 14 universities across Indonesia. The participants worked in teams to develop analytical tools and generate research insights in four areas. During the two research days, researchers explored and analysed the data, guided by image processing and GIS senior researchers as advisors, and representatives from UN OCHA and the National Disaster Management Agency (BNPB) as domain experts on disaster management. The event served as an opportunity for the selected researchers to share their expertise as well as forge networks with decision-makers.

After completing the task during the Research Dive, the four groups submitted extended abstracts, which are presented in this technical report. The first group elaborates on automatic description generation from images related to the haze crisis using deep learning. The second group brings methods to infer the level of visibility from hazy images by applying single-image and learning-based approaches. The third group measures the impacts of volcanic eruption by using spatial data analysis and image processing approaches for satellite imagery data. The fourth group explores the combination of inundation modeling and image mining to portray the relationship between vulnerability and flood inundation.

Pulse Lab Jakarta is grateful for the cooperation of UN OCHA, National Disaster Management Agency (BNPB), Agency for the Assessment and Application of Technology (BPPT), Airlangga University, Bina Nusantara University, Bogor Institute of Agriculture, Gajah Mada University, Hasanuddin University, Khairun University, Lampung University, Sam Ratulangi University, Sebelas Maret University, Tarumanegara University, Telkom University, Trunojoyo University, Udayana University, University of Indonesia. Pulse Lab Jakarta is also grateful for the generous support of the Department of Foreign Affairs and Trade of the Government of Australia, which enabled this research collaboration and many of the Lab's other activities to advance data innovation in development practice and humanitarian action.

January 2017
Pulse Lab Jakarta

Research Dive

Advisors

Dr. Eng. Anto Satriyo Nugroho	Badan Pengkajian dan Penerapan Teknologi
Trias Aditya K. M., ST, M.Sc, Ph.D	Gajah Mada University
Dr. Ir. Agus Wibowo, M.Sc	Badan Nasional Penanggulangan Bencana
Faizal Thamrin	United Nations Office for the Coordination of Humanitarian Affairs

Researchers

Group 1 – Description of Images Related to Haze Crisis in Indonesia Using Deep Learning

Ema Rachmawati	Telkom University
Indah Agustien Siradjuddin	Trunojoyo University
Muhammad Dwisnanto Putro	Sam Ratulangi University
Vina Ayumi	University of Indonesia
Ni Luh Putu Satyaning Paramita	Pulse Lab Jakarta

Group 2 – Inferring the Level of Visibility from Hazy Images

Alexander A S Gunawan	Bina Nusantara University
Heri Prasetyo	Sebelas Maret University
Indah Werdiningsih	Airlangga University
Janson Hendryli	Tarumanegara University
Muhammad Rheza	Pulse Lab Jakarta

Group 3 – Quantifying The Impact of a Volcano Eruption

Dina Chahyati	University of Indonesia
I Dewa Nyoman Nurweda Putra	Udayana University
I Gede Boy Darmawan	Lampung University
Iis Hamsir Ayub Wahab	Khairun University
Imaduddin Amin	Pulse Lab Jakarta

Group 4 – Physical Vulnerability Modeling Based On Flood Inundation Model and Image Mining

Edy Irwansyah	Bina Nusantara University
Guruh Samodra	Gajah Mada University
Hendra Pachri	Hasanuddin University
Maulana Ibrahim Rau	Bogor Agricultural University
Muhammad Subair	Pulse Lab Jakarta

Table of Contents

Research Dive II: Image Mining for Disasters Management

Imaduddin Amin
Pulse Lab Jakarta
Jakarta, Indonesia
imaduddin.amin@un.or.id

Faizal Thamrin
United Nations Office for the Coordination of Humanitarian Affairs
Jakarta, Indonesia
thamrinf@un.org

ABSTRACT
Indonesia is one of the most disaster-prone countries in the world. Recent events include haze from forest fires, volcanic eruptions, floods and landslides. During the Research Dive, 16 academics were invited to work together on imagery data sourced from social media, satellite imagery, and unmanned aerial vehicles (UAVs), to enhance knowledge discovery related to haze, volcanic eruption, floods and landslides. In particular, the task was divided into four tasks; (a) to generate automatic descriptions about the situation during the haze event, (b) to infer the visibility distance during the haze event, (c) to quantify the impact of volcanic eruption, and (d) to create a risk model and assess hazards related to floods and landslides. In order to support participants, Pulse Lab Jakarta, the National Institute of Aeronautics and Space Indonesia (LAPAN), and the National Board for Disaster Management (BNPB) provided imagery datasets.

1. INTRODUCTION
Disasters in Indonesia can be classified into three categories. Firstly, natural disasters such as volcanic eruptions, tsunamis, earthquakes and other nature-caused disasters. Secondly, non-natural disasters such as forest fires and disease outbreaks. Lastly, social disasters including terrorism and conflict.

According to BNPB, the number of disasters in Indonesia is likely to increase every year. In 2015, there were 1,677 disasters recorded, and up to November 2016 there were 1,985 events identified. The top five disaster types include volcanic eruptions, forest fires, floods and landslides.

Indonesia has the most active volcanoes in the world. 75 out of 500 districts in Indonesia are in volcanic risk zones. Approximately 3.85 million people live in these risky areas.

In addition, 274 out of 500 districts in Indonesia are classified as medium-high risk for landslide disasters. Unlike the volcanic eruptions that follow the ring of fire (crossing from Sumatra, Java and the southern part of Indonesia), the landslide risk is scattered across all five main islands in Indonesia and may affect more than 40 million people.

Lastly, forest fires are the largest man-made disaster that happens nearly every year. According to a World Bank report, between June and October 2015, around 100,000 man-made forest fires destroyed about 2.6 million hectares of land and caused toxic haze to spread to other parts of Southeast Asia[1]. Considering the large impact it caused, the event was classified as a regional disaster.

In November 2016, Pulse Lab Jakarta organized a Research Dive, hosting 16 researchers in image processing and Geographic Information System (GIS), to mine and analyse imagery data sourced from social media, satellite imagery, and UAVs related to haze, volcanic eruption, floods and landslides. The objective was to gather valuable information from this data to help authorities improve decision-making and disaster response efforts.

Researchers were given access to 5,400 images related to haze collected from social media, gigabytes of time-series satellite imagery capturing Mount Merapi volcano pre- and post-eruption from LAPAN and Google Earth, and UAV images of the recent landslides in Garut, West Java. The participants were divided into four groups with different tasks; (a) to develop methods for automatic description generation from images related to the haze crisis, (b) to infer the level of visibility from hazy images, c) to quantify the impact of volcanic eruption using time-series satellite imagery, and (d) to model risk and assess hazards related to floods and landslides.

2. DATASETS
2.1. Social Media Data
Pulse Lab Jakarta collected the images related to the haze situation from social media data sources in Haze Gazer (hazegazer.org). To collect these images, we used a set of keywords related to haze such as *kabut asap* (haze), masker (mask) and popular hashtags used during the haze situation such as: #melawanasap (fighting haze), #kabutasap (haze), and #saveriau. This set of keywords is called the taxonomy.

After sending the taxonomy to the application program interface (API) stream, a set of social media messages was returned by the data firehouse. However, not all of the messages were related to the haze; sometimes they contained irrelevant information such as advertising or messages from fake or bot accounts. Thus, we used text processing to filter out non-related haze images.

For the Research Dive, about 5,400 images were chosen randomly from our data collection and were shared with the participants. This included metadata such as the spatial information (latitude, longitude) and temporal information (timestamp) of each image. Out of 5,400 images, we also manually tagged 1,000 images as haze situation pictures and haze context pictures. A picture was tagged as haze situation when it showed the haze conditions such as a gray sky, hazy images and others. Haze context pictures related to the haze but did not necessarily show the haze situation, such as images of people

[1] World Bank. Indonesia economic quarterly: Reforming amid uncertainty; December 2015. Available: http://pubdocs.worldbank.org/pubdocs/publicdoc/2015/12/844171450085661051/IEQ-DEC-2015- ENG.pdf.

wearing masks, a campaign about the haze, and others.

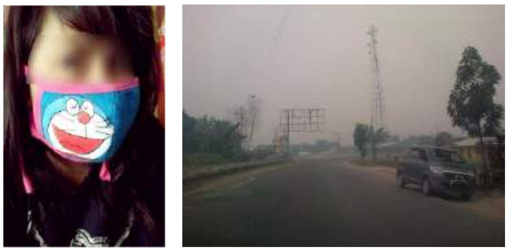

(a) (b)

Figure 1. Images captured from social media, (a) Irrelevant image (non-haze image) and (b) Relevant image

2.2. Un-Georeferenced Images of Mount Merapi

We shared four sets of image collections that show the condition of Mount Merapi in four separate locations. Each collection contained one photo before the eruption, one photo after the eruption and another photo of the current conditions at Mount Merapi. All image sets were captured from Google Earth without the geo-referenced information.

(a) Before eruption

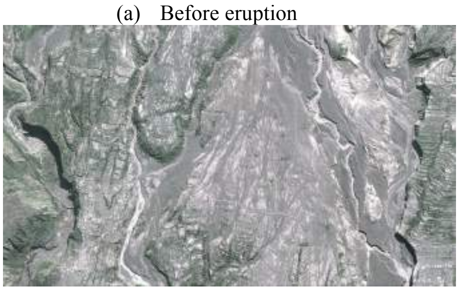

(b) After eruption

(c) Now

Figure 2. Satellite imagery on pre-, post-eruption, and current conditions captured Mount Merapi volcano from Google Earth

Table 1. Meta information on satellite imagery retrieved from Google Earth

Timeseries	Top Left	Bottom Right	Width	Height
Timeseries 1	110°26'20.29"E	7°36'11.00"S	2080 px	1400 px
Timeseries 2	110°27'4.46"E	7°35'36.57"S	2080 px	1400 px
Timeseries 3	110°26'23.01"E	7°35'36.00"S	2080 px	1400 px
Timeseries 4	110°26'9.00"E	7°35'11.82"S	2080 px	1400 px

2.3. Satellite Data

LAPAN provided two sets of data collections based on two locations; Merapi and Garut. LAPAN shared raw data without any preprocessing. The list of satellite files is included in Table [2].

2.4. UAV Data

BNPB provide the UAV data that they used to collect information related to the Garut flash flood and landslides. The UAV had two flight plans on 22 September 2016, at 08.11 GMT+7 and 09.34 GMT+7. Both of the flight plans were located at Tarogong Kaler sub-district and took place just one day after the disaster. Hence, we do not have UAV data capturing the same location before the disaster. Below are the UAV specifications that were used to capture the post-landslide images.

UAV Specifications

Engine (Board)	: Skywalker 2013 Wingspan 1880mm
Servo	: 4 pcs EMAX ES08MAII
Motor	: Sunnysky X2820 800KV
ESC (Electronic Speed Controller)	: Hobbywing Platinum Pro V3 50A
Propeller	: 12 x 6
Battery	: LiPo 4 cells, 5200mAh
Remote Control	: Turnigy 9XR
Camera	: 2.4 GHz 1000 Tx Rx Sony
	: Sony DSC QX 10 18.2 Megapixel
GPS	: Ublox Lea-6H GPS
Telemetry	: RFDesign/RFD900
FPV Monitor	: Fieldview 777
Body Protector	: BEVRC

3. DATA AND TASK MAPPING

At the Research Dive, we defined the research questions along with the datasets. In addition, participants could use their own datasets to answer the research questions.

Social media data was given to the first and second groups. The first group used the image data from social media to classify relevant and irrelevant images related to haze events, and further develop methods to generate automatic description based on the images. The second group used the manually tagged hazy images to infer the visibility level. Un-georeferenced time-series images and satellite imagery of the Mount Merapi volcano area from LAPAN were given to the third group, to quantify the impact of the volcanic eruption. The UAV data and satellite imagery of the Garut area from LAPAN were given to the fourth group, to develop risk models and assess hazards related to floods and landslides.

The researchers invited to the Research Dive are computer scientists with expertise in image processing, and GIS scientists with expertise in remote sensing. The first and second group consisted of computer scientists, while the third group was mixed (computer scientists and GIS scientists) and the last group consisted of GIS scientists.

Table 2. List of satellite imagery data provided by LAPAN

No	Data Type	File Name	Location
1	SPOT5	LPN_SP5_292_365_20140616023050_P_ORT	Garut
2	SPOT5	LPN_SP5_292_365_20140616023053_MS_ORT	Garut
3	SPOT5	LPN_SP5_292_365_20140803020426_MS_ORT	Garut
4	SPOT5	LPN_SP5_293_366_20140803020432_MS_ORT	Garut
5	SPOT6	LPN_SP6_201311010236136_ORT	Garut
6	SPOT6	LPN_SP6_201403040241391_ORT	Garut
7	SPOT7	LPN_SP7_201507170245091_ORT	Garut
8	SPOT7	LPN_SP7_201601080247307_ORT	Garut
9	PLEIADES	TPP1600215150	Garut
10	SPOT4	20091116SP4292365S0G2AXI	Merapi
11	SPOT4	20091116SP4292366S0G2AXI	Merapi
12	SPOT4	20091202SP4293365S0G2AMN	Merapi
13	SPOT4	20100901SP4293365S0G2AXI	Merapi
14	SPOT4	20100901SP4293366S0G2AXI	Merapi
15	SPOT4	20101117SP4292365S0G2AMN	Merapi
16	SPOT4	20101117SP4292365S0G2AXI	Merapi
17	SPOT4	20101204SP4293366S0G2AXI	Merapi
18	SPOT4	20110413SP4292366S0G2AXI	Merapi
19	SPOT4	20110629SP4292365S0G2AMN	Merapi
20	SPOT4	20111111SP4293366S0G2AXI	Merapi
21	SPOT4	20120410SP4292365S8G2AXI	Merapi
22	SPOT4	20120410SP4292366S0G2AMN	Merapi
23	SPOT4	20120410SP4292366S0G2AXI	Merapi
24	SPOT4	20120903SP4293365S0G2AXI	Merapi
25	SPOT4	20120903SP4293366S0G2AMN	Merapi
26	SPOT4	20121009SP4292366S0G2AMN	Merapi
27	SPOT4	20121009SP4292366S0G2AXI	Merapi
28	SPOT4	20111111SP4293365S0G2AXI	Merapi
29	SPOT4	20111111SP4293366S0G2AMN	Merapi
30	SPOT4	20111111SP4293365S0G2AMN	Merapi
31	PLEIADES	FCGC600328615	Merapi
32	PLEIADES	FCGC600328625	Merapi
33	PLEIADES	FCGC600328630	Merapi
34	PLEIADES	FCGC600328704	Merapi
35	PLEIADES	TPP1600215240	Merapi
36	PLEIADES	TPP1600215381	Merapi
37	QUICKBIRD	054830488070_01_P045	Merapi
38	WORLDVIEW2	054830488070_01_P003	Merapi
39	WORLDVIEW2	054830488070_01_P010	Merapi
40	WORLDVIEW2	054830488070_01_P018	Merapi

Description of Images Related To Haze Crisis in Indonesia Using Deep Learning

Ema Rachmawati,
School of Computing, Telkom University
Jl. Telekomunikasi Terusan Buah Batu Bandung, Indonesia
emarachmawati@telkomuniversity.ac.id

Indah Agustien Siradjuddin
Informatics Department
University of Trunojoyo Madura
Telang raya Kamal, Madura, Indonesia
indah.agustien@if.trunojoyo.ac.id

Muhamad Dwisnanto Putro
Jurusan teknik elektro
Universitas Sam Ratulangi
kampus bahu-UNSRAT Manado, Indonesia
dwisnantoputro@unsrat.ac.id

Vina Ayumi
Fakultas Ilmu Komputer,
University of Indonesia
Depok, Jakarta, Indonesia
vinaayumi@gmail.com

Ni Luh Putu Satyaning
PulseLab
Jakarta, Indonesia
ni.paramita@un.or.id

ABSTRACT

Image description for haze images using deep learning method is proposed in this article. The description of haze images which is obtained from the social media is a crucial information for the government, in order to give an early warning for the people about the disaster. There are two main stages applied in this article for describing the content of haze image. First, the selection of the relevant images (haze images), and second, the description of the relevant images. In the first stage, we use histogram of Hue channel as the feature, and Random Forest as the classifier. In the second stage, namely the description stage, we apply the deep learning method, which consist of Convolution Neural Network and Recurrent Neural Network. The images and annotation related to haze crisis are trained using deep learning method. The encouraging experimental results demonstrate that the proposed way to is effective in generating description of images related to haze crisis.

Keywords

Haze Images, Histogram Images, Image Description, Deep Learning, Convolution Neural Network, Recurrent Neural Network.

1. INTRODUCTION

In this study, image description (or popular term commonly used is image captioning) is used to provide a useful description and information of the images, in order to help the Internet users finding images which match their requirements. Sometimes they want to get the exact description of images related to a particular crisis, such as images related to haze crisis. In this case, the image description process is useful for users such as public and government to find information in the form of images related to haze crisis, and at the same time, also accurately match the keywords they typed in the search engines. Hence, the image description allows users to take the images and access them quickly without having to filter and sort the images.

In the image captioning process, we used popular deep learning process, namely CNN (Convolution Neural Network) combined with RNN (Recurrent Neural Network). In the experiment, the training images along with their initial text captions are used in the training process to determine the final caption or description of the test images.

2. IMAGE SELECTION

As the first stage of our proposed method, in this section, we briefly describe the process of getting relevant images from abundant images. The relevant images are images which contain haze-related object or any kind of condition that relate with haze incident (we call it as context-haze) as depicted in Figure 1. Meanwhile the irrelevant images are images which are not related to haze incident at all, as seen in Figure 2.

Figure 1. Relevant Images

Figure 2. Irrelevant Image (non haze Image)

In determining what kind of features which will best differentiate the relevant images from irrelevant images, we conduct histogram analysis to all images. From the analysis, we decide that the best features which distinguish relevant images from irrelevant images are the intensity and the contrast of the images [1], [2]. Therefore, in the selection of relevant and irrelevant image, we use histogram of the image and Random Forest [3] as the classifier in the classification stage. Histogram of the image is considered as the feature for the selection process, since we can distinguish the relevant and irrelevant image from its histogram. The histogram of relevant image tends to assemble in only some level of the histogram, meanwhile in the irrelevant image, the histogram is distributed in almost all level of the histogram.

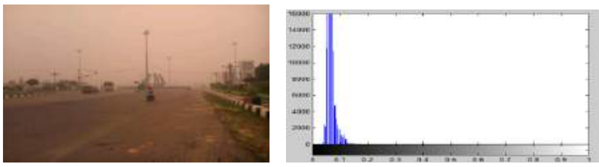

(a)

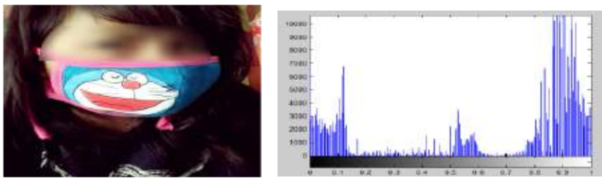

(b)

Figure 3. The histogram of hue value, (a) relevant image (haze image) and (b) irrelevant image (non haze image)

3. IMAGE DESCRIPTION

The second stage of our proposed system is describing the relevant images obtained from previous stage. We adopt the framework of [4] to generate the image description. The model of the image description process is depicted in Figure 4.

As depicted in Figure 4, the description process involved the Computer Vision and Natural Language Processing (NLP). CNN as an image “encoder”, by first pre-training it for an image classification task and using the last hidden layer as an input to the RNN decoder that generates sentences [4].

The CNN used to extract the representation of images. It has been widely used and studied for image tasks, and currently used as state-of-the art for object recognition and detection. The architecture of CNN that we used is GoogleNet [5]. The GoogleNet architecture, the winner of the 2014 ImageNet competition, had 22 layers as shown in figure 4. Along with the input images, we give some initial text caption giving simple description of the input images. The relation of image features and the text caption is processed using Recurrent Neural Network (RNN), in order to generate the description of the image.

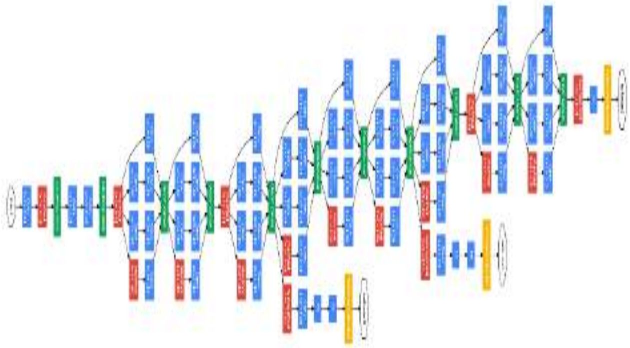

Figure 4. GoogleNet architecture [4]

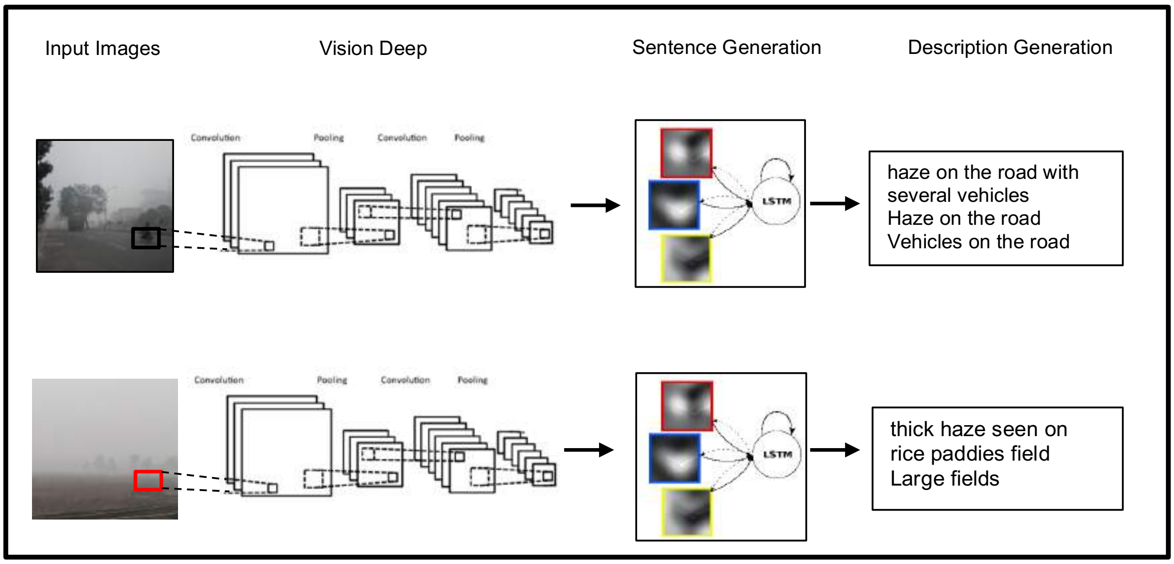

Figure 5. Model of Image Description Process

3.1 Recurrent Neural Network (RNN)

Sentence is comprised of sequence of words, therefore we employ the RNN. RNN is powerful to generate sentence since in the learning process, RNN requires the previous state and the current state of data to predict the output of the neural network. RNN architecture that used in this study is Long-Short Term Memory (LSTM) net, which gives state-of-the art performance on sequence tasks such as translation.

The core of the LSTM model is a memory cell encoding knowledge at every time step of what inputs have been observed up to this step. The behavior of the cell is controlled by "gates" – layers which are applied multiplicatively and thus can either keep a value from the gated layer if the gate is 1 or zero this value if the gate is 0. In particular, three gates are being used which control whether to forget the current cell value (forget gate), if it should read its input (input gate) and whether to output the new cell value (output gate) [4]

4. RESULTS

In the experiment, we use 40 images as training images to generate model. Each image has two or three annotations in the form of simple sentences. The training parameters that used is batch size 100, cnn feature size 1000, embedding size 256, and 20000 iterations. All images are collected from the social media by PulseLab Jakarta. Example of the images and its annotation is shown in Figure 6.

1. Thick haze covers the lake with a bridge
2. Haze on a lake
3. Haze covers a lake with a bridge

1. Thick haze on the road with several vehicles
2. Haze covers the road

Figure 6. Haze images and its annotations for training process

In the testing phase, we use 4 testing images. These images are tested on pretrained model COCO and our trained model. Table 1 shows the result of the experiment.

Table 1. Description of the images from pretrained and trained model

Images	Image Description from pretrained model	Image Description from trained Model
 [image-1]	1. volcano 2. a large bird is sitting on a field 3. a large white bird is parked in the grass 4. a plane is flying in the air 5. a large bird standing on a runway with a tree 6. a large bird standing next to a large field	1. haze on the road 2. haze on the road 3. haze on the road 4. haze on the road 5. haze on the road
 [image-2]	1. a man is riding a motorcycle down a street 2. a man riding a motorcycle down a street 3. a man is riding a skateboard down a street 4. a man sitting on a bench in a parking lot 5. a man is riding a motorcycle down a street	1. wearing a wearing a mask to a for victim 2. several vehicles forest road and a a for victim of haze attack 3. road with several vehicles forest vehicles wearing 4. with several vehicles vehicles a wearing a mask in forest
 [image-3]	1. suspension bridge 2. a plane is flying through a blue sky 3. a large plane that is parked on a runway 4. a large airplane is on the runway 5. a large airplane is flying in the sky 6. a plane is flying on the runway	1. haze on the road 2. haze on the road 3. haze on the road 4. haze on the road 5. haze on the road
 [image-4]	1. mask 2. a man holding a red and a black teddy bear 3. a man is holding a toothbrush to a man 4. a man is holding a white and a kite 5. a man in a bathroom with a skateboard 6. a man holding a white and white umbrella	1. haze on the road 2. haze on the road 3. haze on the road 4. haze on the road 5. haze on the road with several vehicles

The description of the image obtained from COCO's pretrained model shows in the second column of the Table 1. As shown in

Table 1, the description is not well suited with the content of the images. For example, one of the descriptions of the image-3 is 'a plane is flying through a blue sky' and 'a large plane is on the runway'. The image itself looks like a runway, but in this context, this image is about the haze. The result of the same image which is fed into the trained model (using 40 training images) is 'haze on the road'. The description is achieved since the model is trained with the image and annotation related to haze crisis as in Figure 6. Unfortunately, the obtained description is not well structured as seen in the description of image-2, 'wearing a wearing a mask to a for victim' or 'several vehicles forest road and a a for victim of haze attack'. More training images and annotation are required to get a better model.

5. CONCLUSION

The description of images that are related to haze crisis is explained in this article. Firstly, the images are classified into relevant-images and not-relevant-images using histogram of Hue channel as the feature and random forest as classifier. Afterwards, the deep learning method is applied to generate the description of the image. However, the generated description is not well structured since only a few images and annotation are trained in the model. In the further work, we plan to fine tuning the model and use more images and add some annotations along with each image.

6. REFERENCES

[1] X. Yu, C. Xiao, M. Deng, and L. Peng, "A Classification Algorithm to Distinguish Image as Haze or Non-haze," 2011, pp. 286–289.

[2] J. El Khoury, J.-B. Thomas, and A. Mansouri, "Does Dehazing Model Preserve Color Information?," 2014, pp. 606–613.

[3] L. Breiman, "Random Forests," *Mach. Learn.*, vol. 45, no. 1, pp. 5–32, 2001.

[4] O. Vinyals, A. Toshev, S. Bengio, and D. Erhan, "Show and Tell: Lessons learned from the 2015 MSCOCO Image Captioning Challenge," *IEEE Trans. Pattern Anal. Mach. Intell.*, pp. 1–1, 2016.

[5] C. Szegedy, W. Liu, Y. Jia, P. Sermanet, S. Reed, D. Anguelov, D. Erhan, V. Vanhoucke, and A. Rabinovich, "Going deeper with convolutions," in arXiv:1409.4842, 2014.

Inferring the Level of Visibility from Hazy Images

Alexander A S Gunawan
Mathematics Department
School of Computer Science
Bina Nusantara University
Jakarta, Indonesia
aagung@binus.edu

Heri Prasetyo
Informatics Department
Sebelas Maret University
Ir. Sutami No. 36A,
Surakarta, Jawa Tengah 57126
heri.inf.its.02@gmail.com

Indah Werdiningsih
Mathematics Department
Airlangga University
Muljorejo Kampus C
Airlangga University Surabaya
Indah_werdiningsih@yahoo.co.id

Janson Hendryli
Informatics Engineering Department
Tarumanagara University
Letjen S. Parman No. 1
Jakarta, Indonesia 11440
jansonh@fti.untar.ac.id

Muhammad Rheza
Pulse Lab Jakarta
Jakarta, Indonesia
muhammad.rheza@un.or.id

ABSTRACT
In this paper, we provide a brief survey of methods dealing with visibility level of hazy images. The methods is divided into two categories: single-image approach and learning-based approach. The survey begins with discussing single image approach. This approach is represented by visibility metric based on Contrast-to-noise ratio (CNR) and similarity index between hazy image and its dehazing image. This is followed by a survey of learning-based approach. We describe two contrast approaches, that is: (1) based on theoritical foundation of transmission light, combining with the depth image using new deep learning method, (2) based on black-box method by employing convolutional neural networks (CNN) on hazy images and their visual evaluation. We also provide experiments of the representative methods based on social media dataset and comparing the results to visual evaluation of the dataset. This survey is our first attempt to estimate visibility level from social media images.

Keywords
Hazy image; visibility level; single image approach; learning based approach; social media

1. INTRODUCTION
Haze Image occur because bad weather conditions such as haziness, mist, foggy and smoky. The image quality of outdoor scene in the fog and haze weather condition is usually deteriorated by the scattering of a light before reaching the camera due to these large quantities of suspended particles (e.g. fog, haze, smoke, impurities) present in the atmosphere [1]. The presence of haze in the atmosphere degrades the quality of images captured by visible camera sensors. The removal of haze, called dehazing, is typically performed under the physical degradation model, which necessitates a solution of an ill-posed inverse problem [2]. Therefore, improving the technique of image haze removal will benefit many image understanding and computer vision applications such as aerial imagery [3].

We divide the methods to solve the visibility level of hazy image into two categories. First method is only based on single-image, that visibility metric and similarity index. Visibility metric produce a metric based on Contrast-to-noise ratio (CNR). This metric is based on the computation of computation of the standard-deviation image and can be used to judge which dehaze method is better than another one, since it provides a quantitative metric for haze images. The visibility metric is proposed for judging which dehaze method is better [4]. The similarity index is a method for predicting the perceived quality of digital television and cinematic pictures, as well as other kinds of digital images and videos. This index, called as structural similarity (SSIM) [5], is used for measuring the similarity between two images. In here, we compare the original hazy image to dehazing image using SSIM to estimate the visibility level of hazy image.

Second approach is based on learning paradigm. Haze removal is actually a difficult task because fog depends on the unknown scene depth map information. Based physical observation and theory, fog effect is the result of light transmission and distance between camera and object. Hence removal of fog requires the estimation of airlight map [1]. Furthermore, Jian Sun et al [2] found that there are dark pixels whose intensity values are very close to zero for at least one color channel within an image patch, called as dark channel. Approximation to zero for the pixel value of the dark channel is called the DCP [4]. The dark channel prior is based on the statistics of haze-free outdoor images. Combining a haze imaging model and a soft matting interpolation method, we can recover a hi-quality haze-free image. By using a transmission matrix generated from dark channel prior algorithm [2], and the depth map from new Deep Convolutional Neural Fields (DCNF) method [7], haze level score can be computed by combining the transmission matrix and depth map. Depth estimation is estimate depths from single monocular images [7]. We consider the transmission matrix as the perceived depth of hazy photos, which is a combination of actual depth and haze effects. Therefore, by ruling out the actual depth factor, we can isolate the haze effects from the transmission matrix, which is used to estimate the haze level [5]. Recently, there is evidence that the black-box approach using deep convolutional neural networks (CNN) are setting new records for various vision applications. To consider this black-box approach, we also create convolutional neural networks (CNN) based on hazy images and their visual evaluation.

We propose visibility metric, similarity index, theorical approach based on transmission and depth map and black-box approach based on CNN. The experiment will compare the results these four approaches.

2. SINGLE IMAGE APPROACH

In single image-based approach, we infer the haze visibility level only by one image through image processing techniques, such as visibility metric and image similarity index which explain in detail in next subsection.

2.1 Visibility Metric

The visibility metric is based on the computation of the standard-deviation image and can be used to judge which dehaze method is better than another one, since it provides a quantitative metric for haze images. This visibility metric is calculated by using Contrast-to-Noise Ratio (CNR) [5] of noise image estimated by Gaussian kernel. Contrast-to-noise ratio (CNR) is a measure used to determine image quality. CNR is similar to the metric, signal-to-noise ratio (SNR), but subtracts off a term before taking the ratio. This is important when there is a significant bias in an image, for example in hazy image which the features of the image are washed out by the haze. Thus this image may have a high SNR metric, but will have a low CNR metric. We experiment with the visibility metric from Zhengguo [4].

2.2 Stuctural Similarity Index

The structural similarity (SSIM) index [5] is a method for predicting the perceived quality of digital television and cinematic pictures, as well as other kinds of digital images and videos. It was first developed in the Laboratory for Image and Video Engineering (LIVE) at The University of Texas at Austin and in subsequent collaboration with New York University. SSIM is used for measuring the similarity between two images. The SSIM index is a full reference metric; in other words, the measurement or prediction of image quality is based on an initial uncompressed or distortion-free image as reference. SSIM is designed to improve on traditional methods such as peak signal-to-noise ratio (PSNR) and mean squared error (MSE), which have proven to be inconsistent with human visual perception.

To estimate the visibility level of hazy image, we compare the original hazy image to dehazing image using SSIM. In order to utilize SSIM, one renown image dehazing method, called as multi-scale fusion algorithm [9], is used to do haze removal

2.2.1 Single Image Dehazing based on Multi-scale Fusion

Haze is an atmospheric phenomenon that significantly degrades the visibility of outdoor scenes. This is mainly due to the atmosphere particles that absorb and scatter the light. For our experiment, we used muti-scale fusion algorithm for removing have in an image. This fusion-based strategy works by applying a white balance and a contrast enhancing to two original hazy image inputs.To blend effectively the information of the derived inputs to preserve the regions with good visibility, we filter their important features by computing three measures (weight maps): luminance, chromaticity, and saliency (see Figure 1). To minimize artifacts introduced by the weight maps, it is designed in a multiscale approach, using a Laplacian pyramid representation. The implementation of multi-scale fusion algorithm is appropriate for real-time applications [10].

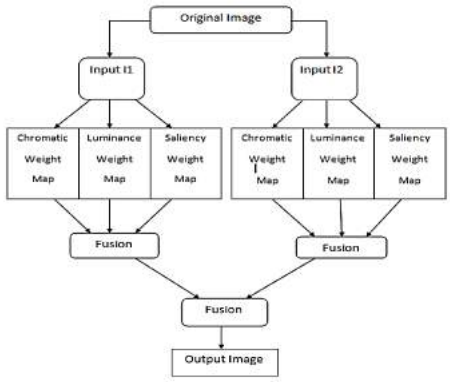

Figure 1. Multi-Scale Fusion Algorithm

The below procedure [11] is foundation of the multi-scale fusion algorithm, that is:

1) Derive two input images from the original input with the aim of recovering the visibility for every region of the scene in at least one of them. a) First input will be obtained by applying white balancing. b) Second input will be obtained by applying contrast enhancement technique.
2) Compute 3 weight maps such as luminance, chromaticity and saliency and weight the derived inputs by 3 normalized weight maps.
3) Apply multi-scale fusion, utilizing Laplacian pyramid delegation of inputs blended along with Gaussian pyramids of normalized weights to obtain the haze free image.
4) Apply Unsharp Masking method (USM) for image dehazing on original hazy input image to obtain the haze free image.
5) Compare the results of single image dehazing using multi-scale fusion method with Unsharp Masking method of single image dehazing to prove the efficiency of Unsharp Masking method.

3. LEARNING-BASED APPROACH

In contrast to single image approach, learning-based approach envoy a model learned from many images to help inferring the haze visibility. In here, we employ two contrast approaches, that is: (1) based on theoritical foundation of transmission light, combining with the depth image using new deep learning method, (2) based on black-box method by employing deep learning on hazy images and their visual evaluation. Therefore, there are two learning-based approaches that we use in this research: Deep Convolutional Neural Fields (DCNF) to learn depth from images and Convolutional Neural Network (CNN) to classify haze level into two classes of heavy and light haze

3.1 Depth Map and Transmission Matrix

The basic idea of this approach is that the haze visibility can be inferred by computing the depth of the images and the transmission matrix generated from a haze removal algorithm. In paper [8], Li et al proposed a framework to estimate haze level from a photo by using the Dark Channel Prior (DCP) [2] to estimate the transmission matrix and the deep convolutional neural fields (DCNF) [7] to estimate the depth map. By combining this information, they select from a combination of transformation and pooling functions to estimate the haze level. Figure 2 shows the proposed framework of [8].

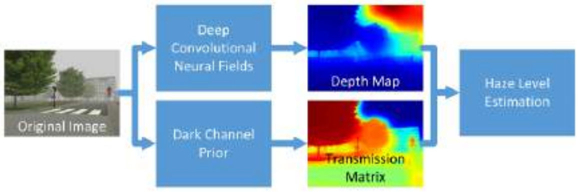

Figure 2. The proposed framework of [8] to estimate the haze level from photos

The DCNF is proposed by [7] to estimate depth information given a single monocular image. The model combine the strength of convolutional neural network (CNN) and conditional random fields (CNF) to predict the depths. Experimental results from [7] shows improved accuracy on various dataset and other baseline methods. Figure 3 below shows the illustration of the DCNF model. For the DCNF, we use the source code and learned model provided by the authors[1].

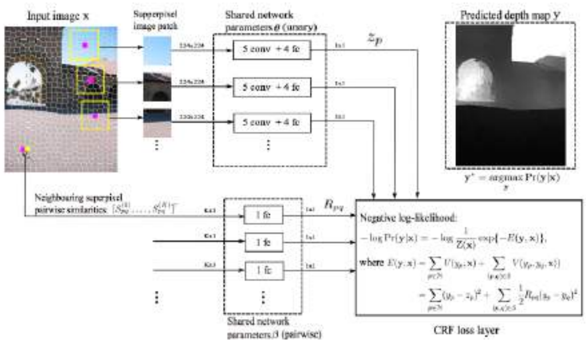

Figure 3. Deep Convolutional Neural Fields (DCNF) model [7]

Our approach is quite similar to [8], but we choose to use following equation to estimate the haze level from the estimated depth map and transmission matrix:

$$k = \text{median}\left(\frac{\log t(x)}{d(x)}\right) \quad (1)$$

where k denotes the haze level, $t(x)$ is the transmission matrix, and $d(x)$ is the depth map. Our choice of transformation and pooling function are due to the time and computation constraint.

3.2 Convolutional Neural Network

Convolutional Neural Network (CNN) was another approach we experimented on. Nowadays, CNN has been arguably the best image classifier since Krizhevsky, et al. won the ImageNet object classification in 2012 using deep CNN [12]. CNN is basically a feed-forward neural network but with a convolutional layer for the purpose of learning the best representation of the images. Early implementation of CNN, widely known as LeNet-5 [13], applied by several banks to recognize handwritten digits on cheques.

[1] https://bitbucket.org/fayao/dcnf-fcsp

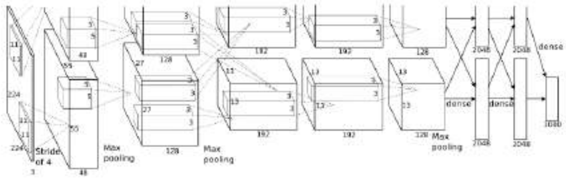

Figure 4. Architecture of AlexNet [12]

Figure 4 shows the architecture of Krizhevsky's deep CNN, widely known as AlexNet, that won the ImageNet challenge on 2012. The networks consist of 5 convolutional layers, followed by 3 layers of fully-connected networks. On the first, second, and fifth convolutional layers, a max-pooling layer is applied to summarize the outputs of adjacent neurons in the same layer [12]. In addition to that, it applies the ReLU activation functions to the output of every convolutional layer. Finally, the last layer is a softmax which produces a distribution over the 1000 class labels. Moreover, a dropout regularization is used in the first two fully-connected layers to reduce overfitting. The AlexNet model is trained using Stochastic Gradient Descent (SGD) with a batch size of 128, momentum 0.9, and weight decay of 0.0005.

We implement our CNN to classify hazy images into two classes of heavy haze and light haze using Keras and Python. Our network consists of 6 layers, of which 3 layers are the convolutional layers and 3 layers are the fully-connected. We use max-pooling of size 2 x 2, ReLU activation on each convolutional layers, and a dropout regularization on the first and second fully-connected layers. The output of the last layer is fed to a sigmoid function. We also train the network using SGD with a batch size of 32 and 100 epoch. Furthermore, image augmentations are applied to each training images, which rotate, translate, rescale, zoom, and horizontally flip the images to reduce overfitting. The augmentations are performed using Keras ImageDataGenerator library. Figure 5 below illustrates the configuration of our CNN model.

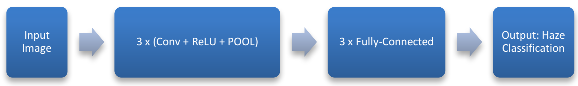

Figure 5. Architecture of our CNN model to classify haze level

4. EXPERIMENT RESULTS

4.1 Datasets

For CNN, we manually classify the data from social media provided by Pulse Lab Jakarta into two classes of haze level: heavy and light. We obtain 300 images for training (191 images for heavy haze and 109 images for light haze) and 57 images for testing. Furthermore, we test the CNN model with 5 additional images with higher resolution. Since the social media images where the dataset comes from are heavily filtered i.e. Instagram filters, we need to test the robustness of the model using non-social media images. These additional images are retrieved from simple Google search of haze images.

4.2 Experiments on Single Image Approach

Visibility metric (VM) estimate how far visibility level based on single image. Thus lower VM should represent thicker haze. The result of VM on Pulse Lab hazy images dataset can be seen in Figure 7 below. VM is only suitable to compare the same outdoor images with different haze level, so VM is not too reliable in estimating visibility level of many unrelated outdoor images taken from social media. On the other hand, structural similarity (SSIM) index is based on comparison of original hazy image and its dehazing image. Therefore, SSIM is depended on the dehazing image algorithm. For our experiment, we choose recent multi-scale fusion algorithm [9]. Because SSIM essentially measure similarity distance, then larger SSIM should represent thicker haze. The result of SSIM on Pulse Lab hazy images dataset can be seen in Figure 7 below.

4.3 Experiments on Learning-based Approach

The result of running DCNF on Pulse Lab hazy images dataset can be seen in Figure 6 below. The heat map should be corresponding to the distance between the objects on the images and the camera. As we can see from the figure, the depth map has troubled inferring the depth of the sky and heavy haze-covered objects. Calculating haze level k using Eq. 1 gives us results shown in Figure 7. The transmission matrices *t(x)* used in this approach come from Dark Prior approach [2]. The larger value of k should mean the haze is heavier, though there are some inaccuracies. For example, for Figure 7 (c), the value of k is larger than 7 (d), in spite of the heavier haze level that can be seen visually.

(a) (b)

(c) (d)

Figure 6. Result of DCNF on Pulse Lab dataset. Images pair (a)-(b) and (c)-(d) show the original images and the corresponding depth map.

VM=31.7657	VM=28.4074	VM=50.2235
SSIM=0.4141	SSIM=0.6229	SSIM=0.6042
k = 0.022964	k = 0.027969	k = 0.031128
(a)	(b)	(c)

VM= 31.2852	VM=41.2091	VM= 21.0301
SSIM= 0.7515	SSIM= 0.7964	SSIM=0.5256
k = 0.029282	k = 0.032166	k = 0.04007
(d)	(e)	(f)

Figure 7. Estimated haze level SSIM, k using DCNF and transmission matrix. Larger SSIM and k represent thicker haze, but lower VM should represent thicker haze

Figure 8 below shows the classification of the 5 additional high-resolution images using CNN model, trained on 300 social media images provided by Pulse Lab Jakarta. The CNN model correctly classifies the heavy haze images, illustrated in Figure 8 (d) and (e), although (c) can be argued as light or heavy haze. It can be concluded that the CNN specifically recognize the heavy haze images from the visibility level of objects in an image. For the Pulse Lab dataset, we get around 0.75 accuracy though the training epoch hasn't really converged due to the time constraints.

(a) (b) (c)

(d) (e)

Figure 8. CNN classification result of the 5 additional images. Images (a)-(c) are classified as light haze, while images (d) and (e) are correctly classified as heavy haze.

In this study, we have evaluated several method for estimating visibility level that is: visibility metric (VM), structural similarity (SSIM), the depth map + dark channel prior (DCNF+DCP), and convolotional neural network (CNN). To make brief comclusion, we calculated Spearman correlation index like in [8] based on the experiment results and human expert evaluation of Pulse Lab hazy images dataset. Unfortunately, CNN classification approach does not give any value to represent visibility level, so we can not calculate its correlation index.

Table 1. Spearman correlation coefficients (%) performance

VM	SSIM	DCNF + DCP	CNN
-0.29	-0.08	0.66	-

Furthermore in our short time experiment, we managed to train 6 layers of CNN and got the 75% classification accuracy which looks so promising. In this training, the CNN model hasn't converged well. Yet, validation on additional 5 images with higher resolution gives arguably good results. The hyperparameters of the CNN can also be fine-tuned more i.e. by choosing better layer configuration. Furthermore, mean normalization can be used for the input images, so hopefully, the loss functions can converge more quickly and we could get the best model to predict the haze level from images. The hyperparameters of the CNN can also be fine-tuned more i.e. by choosing better layer configuration. Furthermore, mean normalization can be used for the input images, so hopefully, the loss functions can converge more quickly and we could get the best model to predict the haze level from images.

5. CONCLUSION

We managed to experiment on several approaches to estimate visibility level in the restricted time. Based on correlation coefficient (see Table 1), the DCNF + DCP approach gives most promising result. It's correlation comparing to human expert evaluation reaches 66%, but there are still some inaccuracies. We argue that the problem is on the quality of depth map produced by the DCNF. Due to the unavailability of ground truth depth map for Pulse Lab dataset, we cannot train the DCNF to predict the depth from the provided dataset. Moreover, the dataset contains various filtered processing and low-resolution images, that the visibility level model is incorrectly estimated. The DCNF should be trained on social media images i.e. Pulse Lab dataset to be able to model the variability of image resolution and quality. The problem is the depth information of the dataset is not readily available. The other approaches (VM, SSIM) seems only suitable for just well-behaved image dataset, and not to fit for ill-behaved social media image dataset.

6. ACKNOWLEDGMENTS

We would like to thank to Pulse Lab Jakarta for introduce us to the problem discussed in this paper, as well as for provides data used in this experiment.

7. REFERENCES

[1] M. K. Saggu and S. Singh, "A Review on Various Haze Removal Techniques for Image Processing," *International Journal of Current Engineering and Technology* , vol. 5, no. 3, pp. 1500-15005, 2015.

[2] K. He, J. Sun and X. Tang, "Single Image Haze Removal Using Dark Channel Prior ,," in *Computer Vision and Pattern Recognition 2009 IEEE Conference*, Florida, 2009.

[3] G. Woodell, D. J. Jobson, Z.-u. Rahman and G. Hines, "Advanced image processing of aerial imagery, Vis. Inf. Process. XV 6246 (2006) 62460E.T," in *Visual Information Processing XV, 62460E*, 2006.

[4] D. Zhengguo, "A New Visibility Metric For Haze Images," MathWork, Dai zhengguo. [Online]. Available: https://www.mathworks.com/matlabcentral/fileexchange/33529-a-new-visibility-metric-for-haze-images.

[5] Z. Wang, A. C. Bovik, H. R. Sheikh and E. P. Simoncelli, "Image quality assessment: From error measurement to structural similarity," *IEEE Transactions on Image Processing,* vol. 13, pp. 600--612, 2004.

[6] S. Lee, S. Yun, J.-H. Nam, C. S. Won and S.-W. Jung, "A review on dark channel prior based image dehazing algorithms," *EURASIP Journal on Image and Video Processing,* vol. 4, 2015.

[7] F. Liu, C. Shen and G. Lin, "Deep Convolutional Neural Fields for Depth Estimation from a Single Image," in *IEEE Conference on Computer Vision and Pattern Recognition*, Boston, 2015.

[8] Y. Li, J. Huang and J. Luo, "Using User Generated Online Photos to Estimate and," in *International Conference on Internet Multimedia Computing and Service (ICIMCS 2015)*, 2015.

[9] C. O. Ancuti and C. Ancuti, "Single image dehazing by multi-scale fusion," *IEEE Transactions on Image Processing ,* vol. 22, no. 8, pp. 3271 - 3282, 2013 .

[10] S. A. M, "Single Image Dehazing using multiple fusion technique," MatWorks, [Online]. Available: https://www.mathworks.com/matlabcentral/fileexchange/47147-image-dehazing-zip.

[11] N. Padole and A. Khare, "Improved Method of Single Image Dehazing based on Multi-Scale Fusion," *International Journal of Computer Science and Information Technologies,* vol. 6, no. 3, pp. 2945-2949, 2015.

[12] A. Krizhevsky, I. Sutskever and G. E. Hinton., "Imagenet classification with deep convolutional neural networks," *Advances in Neural Information Processing Systems,* vol. 1, p. 1097–1105, 2012.

[13] Y. LeCun, B. Boser, J. S. Denker, D. Henderson, R. E. Howard, W. Hubbard and L. D. Jackel, "Backpropagation applied to handwritten zip code recognition," *Neural computation,* vol. 1, no. 4, pp. 541-551, 1989.

Quantifying The Impact of a Volcano Eruption

Dina Chahyati
Computer Science Department
Universitas Indonesia
Jakarta, Indonesia
dina@cs.ui.ac.id

I Dewa Nyoman Nurweda Putra
Marine Fisheries Department
Udayana University
Bali, Indonesia
nurweda14@unud.ac.id

I Gede Boy Darmawan
Geophysics Department
Lampung University
Lampung, Indonesia
igedeboy@staff.unila.ac.id

Iis Hamsir Ayub Wahab
Electrical Engineering Department
Khairun University
Ternate, North Maluku, Indonesia
hamsir@unkhair.ac.id

Imaduddin Amin
Pulse Lab Jakarta
Jakarta, Indonesia
imaduddin.amin@un.or.id

ABSTRACT
In this research, we try to quantify the impact of a volcano eruption using spatial data and time-series images captured from satellite imagery data. We divide the task into two parts. First, a macro analysis approach to prioritize area using spatial data. Second, we quantify the number of damage and recovery part using image processing approach. By using the spatial data, we are able to detect the distribution of the impact of the eruption as well as areas that have been recovered after the eruption on a broad scale and by using the image processing approach we are able to identify the land-use changes as well as quantify the number of damage such as the sand river expansion and the number of destroyed and recovered building.

Keywords
Change detection; eruption; image processing, spatial data

1. BACKGROUND
Merapi volcano (Central Java, Indonesia) is one of the world's most active and dangerous volcanoes. It contains an active lava dome which regularly produces pyroclastic flows. In late October and early November 2010, the mount Merapi's eruption. This disaster caused 9 villages are destroyed and over 350.000 people were evacuated. The volcano eruption is different from other natural disasters because it was in areas remain. Therefore, to determine the impact of a wide range of volcanic eruptions can be done using remote sensing applications.

Remote sensing can monitor the volcano in the most remote areas. The ability to collect data directly from satellites today has increased the timely study of volcanic eruptions. By using remote sensing, it is possible to measure the effects of volcanic eruptions on the surface (Fernández L, Álvarez G, Salinas R., 2012). Ortiz (1996) has conducted studies to prove the multi deformation pre-eruption disorders, post-eruptive and assess the impact of the eruption. However, the remote sensor depends on the bandwidth and radiometric resolutions are not capable of detecting this change in surface or, in other words, change the terrain texture (Haralick R, Shanmugam K, Dinstein I., 1973).

In this research, we try to quantify the impact of a volcano eruption by investigate the landsat use. According to authorities, the merapi area can be classified into several classes such as forest, paddy field, livestocks, housing, sand river, open area. In this research the classification class is selected by combining similar area into same class.

Four main class was selected for this research, such as;

1) Vegetation, includes forest and paddy field
2) Building, includes the livestocks and housing
3) Sand River, and
4) Open area

We select two main tracks for this research such as:

1) Macro analysis approach that prioritize impacted area by looking at the Spatial data. This tracks aims to give an information to authority to take action immediately during the disaster
2) Detail analysis to quantify impact using image processing approach. This tracks aims to give an information to authority about the land-use changes in number such as the area and number of damaged building. By implementing the same approach for the data years after the eruption, this method is also can be used to quantify the recovery area.

2. RELATED WORK
In the event of a natural disaster, remote sensing is a valuable source of spatial information and its utility has been proven on many occasions around the world. However, there are many different types of hazards experienced worldwide on an annual basis and their remote sensing solutions are equally varied (Joyce et al. 2009). Jiménez-Escalona, Granados, & Realmuto (2011) use satellite MODIS images as tools for monitoring the volcano activities emissions. From This study, it was possible to determine three cases related to volcanic ashes. The three of classes are 1) follow up of volcanic ash and gases transported by wind, 2) calculation of ash-cloud residence time in the atmosphere, 3) effects of shearing winds during the ascent of an ash plume.

Moreover, SPOT XS and Panchromatic images is used jointly in order to map the lava flows of the Nevado Sabancaya volcano (southern Peru) (Legeley-Padovani et al. 1997). The unsupervised multispectral clustering applied to the XS image and some specific methods of image analysis using mathematical morphology and convolution filtering applied to the Panchromatic image for produce of map impact of lava volcano. The resulting is allowed to identify flows and the two main morphological features of the flow areas i.e. lava reliefs and flow lines.

Advanced Spaceborne Thermal Emission and Reflection Radiometer (ASTER) is an advanced multispectral imager that was launched on the NASA spacecraft, satellites in Earth Observing System (EOS) TERRA named in December 1999. ASTER covers a wide spectral region with 14 channels consisting of three sensors. The sensor is VNIR (Visible and Near Infrared) consists of 3 channels, SWIR (Short Wave Infrared) consists of 6 lines and TIR (Thermal Infrared) consisting of 5 channel. For VNIR channel has a spatial resolution of 15 m, SWIR has a spatial resolution of 30 m and TIR has a spatial resolution of 90 m, each ASTER image covers an area of 60 x 60 km (Abrams et al., 2002).

Volcano hazards monitoring, geology and soil mapping are specific applications for which ASTER was developed. The easy availability, low cost and unique combination of multispectral and 3D capabilities at 15m resolution are the main advantages of ASTER for volcano study (Kervyn et al, 2007).

Wiart et al. (2000) proposed image processing techniques were tested i.e. principal component analysis (PCA) and optical-SAR for estimate the volumes of lava flows erupted and the timing of explosive and effusive activity of Dubbi volcano. SAR imagery revealed old lava flows buried below tephra deposits, emphasizing the ground penetrating property of the L-band (HH polarization). Two scenarios are identified as a bimodal basaltic-trachytic eruption, with a minimum volume of 1.2 km3 of hawaiite lava and a minimum area of 70 km2 of trachytic pumice; it represents the largest known historic eruption in the Afar triangle. The interpretation obtained from satellite imagery was cross-checked with sparse historical testimonies and available ground-truth data.

Walter et al. (2013) present the results from an analysis of nighttime time-lapse infrared images and compare these data with local seismic amplitude recordings. Images taken before and after the explosions reveal the location of the hot dome to be subject to significant and systematic lateral pixel offsets. Therefore, the analysis of the infrared image correlation suggests the occurrence of aseismic dome-deformation episodes, thereby challenging the current understanding of dome growth and/or the appropriateness of commonly used volcano surveillance techniques.

3. METHOD AND RESULT

3.1 Analysis for Georeferenced Imagery

The image data used are ASTER Imagery which freely available and time series from the AVA (ASTER Volcano Archive). This ASTER image given in HDF format and at the L1B level by the number of scene as much as 8 consisting of 3 VNIR (Visible Near Infra Red) channel and 5 TIR (Thermal Infra Red) channel. In this study, three images used with the time of acquisition is before the eruption in 2009, when the eruption occurred in 2010 and after the eruption in 2012. Particularly in this study, we used only VNIR channel of ASTER Image.

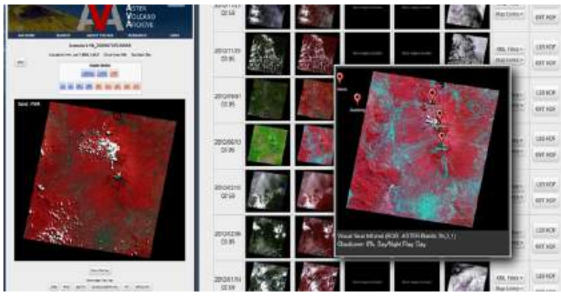

Figure 1. Multi-Scale Fusion Algorithm

3.2 ASTER Image Preprocessing

In the utilization of ASTER image, pre-processing is required to obtain surface reflectance values. This value is derived from the conversion of DN by applying some of the parameters that exist in the metadata. The parameters available in the metadata includes the time of acquisition, the conversion coefficient value of each channel, and angle of azimuth and angle of solar radiation. This parameter to be a reference in the preprocessing stage.

On the stage of the conversion DN to radiance value, the equation used is advanced by Abrams, *2000* $L_\lambda = (DN - 1) \times$ *Unit Conversion Coefficient*. The following is a table of unit conversion coefficient by Abrams, 2000.

Table 1. ASTER unit conversion coefficient by Abrams, 2000

Band No.	Coefficient (W/(m^2*sr*μm)/DN)			
	High gain	Normal Gain	Low Gain 1	Low gain 2
1 2 3N 3B	0.676 0.708 0.423 0.423	1.688 1.415 0.862 0.862	2.25 1.89 1.15 1.15	N/A
4 5 6 7 8 9	0.1087 0.0348 0.0313 0.0299 0.0209 0.0159	0.2174 0.0696 0.0625 0.0597 0.0417 0.0318	0.290 0.0925 0.0830 0.0795 0.0556 0.0424	0.290 0.409 0.390 0.332 0.245 0.265
10 11 12 13 14	N/A	6.822×10^{-3} 6.780×10^{-3} 6.590×10^{-3} 5.693×10^{-3} 5.225×10^{-3}	N/A	N/A

The conversion produces radiance values from VNIR Band of ASTER image and we have to convert this radiance to reflectance value. To conduct this stage, we need the information of acquisition time to determine the Earth-Sun distance. The Earth-Sun distance is derived by taking the Calendar date of the scene and converting it to a Julian date and then calculating the distance. The following are part of Earth-Sun distance table.

Table 2. Earth – Sun Distance in Astronomical Units (Chander and others, 2003)

DOY	Distance	DOY	Distance	DOY	Distance
1	0.9832	121	1.0076	242	1.0092
15	0.9836	135	1.0109	258	1.0057
32	0.9853	152	1.0140	274	1.0011
46	0.9878	166	1.0158	288	0.9972
60	0.9909	182	1.0167	305	0.9925
74	0.9945	196	1.0165	319	0.9892
91	0.9993	213	1.0149	335	0.9860
106	1.0033	227	1.0128	349	0.9843
DOY- Day of Year (Julian Day)				365	0.9833

Moreover, there is an attribute called "SOLARDIRECTION" in the ProductMetadata.0 group in the embedded HDF metadata. It defines the sun direction as seen from the scene center. For example:

OBJECT	= SOLARDIRECTION
NUM_VAL	= 2
VALUE	= (177.154016, 32.061355)
END_OBJECT	= SOLARDIRECTION

The second value (32.061355) is the Elevation angle in degrees (values can range between <= -90.0 to <= 90.0).

The last parameter is the value of irradiance on ASTER image of each channel. This value is obtained from Thome and others, 1998 as shown in the table below,

Table 3. ASTER Solar Exoatmospheric Solar Irradiances (modified from Thome and others, 1998)

ASTER Band	Spectral Irradiance: Modtran-Based ($W/m^2/\mu m$)
1	1848
2	1549
3	1114
4	225.4
5	86.63
6	81.85
7	74.85
8	66.49
9	59.85

by applying all the parameters and attributes from the metadata on each ASTER image, then the value of radiance imposed following equation:

$$P_\lambda=(\pi \times L\_\lambda \times d\text{^}2\ )/(Irradiance \times \sin(\pi \times sun\ elevation\ angle/180)$$

whole VNIR band from ASTER image must be converted into the reflectance values. By obtaining the reflectance value, the last stage of preprocessing is correcting the area of cloud cover and shade.

To get a formula that can detect the reflectance values of clouds and shadows on ASTER image automatically, then the histogram analysis performed on each band. Based on the analysis histogram, obtained that the band two (2) able to detect the area of cloud reflectance. The formula is *Cloud ≥ mean of Band2 +2stdev* and this formula applied to be the threshold values for the cloud. The whole area which covered by clouds corrected by changing its reflectance value become NoData.

3.3 Classify the Image Into Classes from Histogram Analysis

To classify the reflectance values that have been corrected in the previous process, the histogram analysis is required to obtain a threshold value from each reflectance representing several classes of vegetation, lava or laharic flows (volcanic eruption product), buildings and open areas. The following are some of the steps taken in the classification of these classes:

1) Using vegetation index method in separating between the reflectance of vegetation (Veg) or non vegetation ($Nveg$). The threshold values used to separate vegetation and non vegetation is based on the equation $NDVI = \frac{NIR - RED}{NIR + RED}$ and $Veg = NDVI + stdev$ alse is $Nveg$.

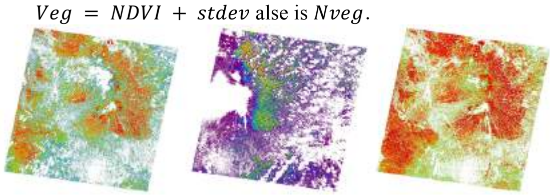

Figure 2. Vegetation Coverage from ASTER datasets

2) To obtain the expected area as lava or rock outcrops, then carried back to the $Nveg$ histogram analysis so that the resulting formula as follows:

$$Lava = ((NIR < (mean - stdev)\ \&\ RED > (mean - stdev))\ ||\ ((NIR < (mean - stdev)\ \&\ Nveg < (mean - 2stdev))$$

the results of the threshold value of the formula is expected as the area of outcrop of volcanic rock or lava while beyond that value is assumed as an open area including buildings.

3) Across the threshold value of the histogram analysis classified into a class of its own with a unique pixel value created. The value of the cloud cover is NoData, vegetation is 2, the open area is 3 and the lava is 5.

Based on the results of the application of the formula and the classification of the three ASTER datasets then acquired land cover classes as shown by the following figure:

Figure 3. Land cover classification ASTER image before (2009), when (2010) and after the eruption (2012)

3.4 Quantify the Impact of Eruption

To identify the impact of the eruption on this research can be done by performing numerical calculations on land cover data that has been given a unique pixel value. Changes in land cover due to volcanic eruption may be identified by several factors such as changes in the vegetation into the open area. These changes can be demonstrated by detection of changes shown by the following figure.

Figure 4. Change detection result of ASTER before and during eruption as well as during and after the eruption

In addition to the change detection method, other numerical method used is by subtracting the data before the eruption to the data after the eruption in order to obtain the classification of negative values is assumed to be the region / area affected by volcanic or by humans. The results of the analysis of the impact of the eruption is shown by the following figure.

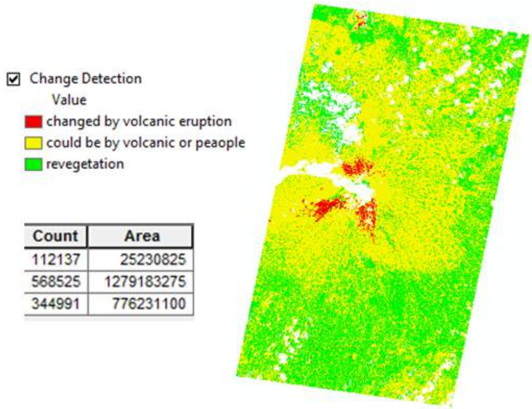

Figure 5. Detection of the impact of eruption based on ASTER data before to the when eruption

Red and yellow areas are the areas affected by volcanic eruptions and centered around the central zone of the crater. Nonetheless, some correction factor needs to be done especially in the areas far from the central zone which also gives a yellow color response. It can be caused by factors determining the accuracy wrong due to the threshold value is less accurate and also due to the reflectance values that are similar, or too distracted. Therefore additional correction data is needed such as topography / geomorphology of volcanic and correcting the distance from the central zone and proximal to the volcanic crater.

In addition to quantifying the area affected by the volcanic eruption, this data can also be used to analyze the areas that have been recovered, especially in terms of the recovery of the vegetation. By utilizing numerical operations, namely the reduction between the current data with the data after the eruption eruption resulting in a positive value is assumed to be a change from the open area and lava into the vegetation. Areas which is positive is defined as an area that has been recovered mainly vegetation as shown by the following figure.

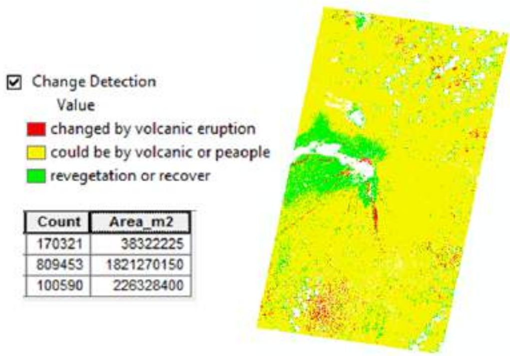

Figure 6. Detection area that has been recovered based on ASTER data when the eruption to after eruption

Green area shows the change from the open area and lava into the vegetation. The condition of this area is located near the central zone of volcanic craters indicate areas that have been recovered due to the eruption. In addition, the pattern of the laharic flow are also visible change with the direction of flow of the main river, so it can be estimated that the area of the main river channel is still prone to lahars flood.

3.5 Analysis for Un-Georeferenced Imagery

The images used in this analysis are satellite imagery taken by Google. These images are not georeferenced as we screenshot the images from Google Map as ordinary image files and thus the coordinates information are lost. The image set consists of three images: Before (before eruption happened), After (right after the eruption), Now (about 4 years after eruption).

3.5.1 Land Cover Classification

Visually we can recognize the four class in the image by using their color only, and thus we don't use other features such as texture. The color space that we use is RGB. The classification steps are:

1) Take some sample patch of each class from the images
2) Calculate the mean RGB for each class as class representative (m_1, m_2, m_3, m_4)
3) For each pixel x in the image:
    a. Take n by n neighboring window centered at pixel x. We tried taking 3,5,7 or 9 as n, and find that n = 5 gives best result.
    b. Calculate m_x the mean of these neighboring pixel.
    c. Calculate the distance between the m_x to (m_1, m_2, m_3, m_4) using Euclidean distance.
    d. Assign x to class i if the distance between m_x and m_i are the minimum.

One problem that we encounter when using this method is color range similarity between classes, as shown in Figure 1 where building's color is similar to sand river (in Before.png). Fortunately, the two class have different size. So in this case, we solve the problem by doing two step processing, such as:

1) Classify building and sand river as same class.
2) Separate building and sand river by their size. We use connected components in this process and define sand river as objects whose size is greater than the threshold (25.000 pixels).

The same problem happens in Now.png, where the color of sand river is now similar to open area. We use the same processing step and get good results.

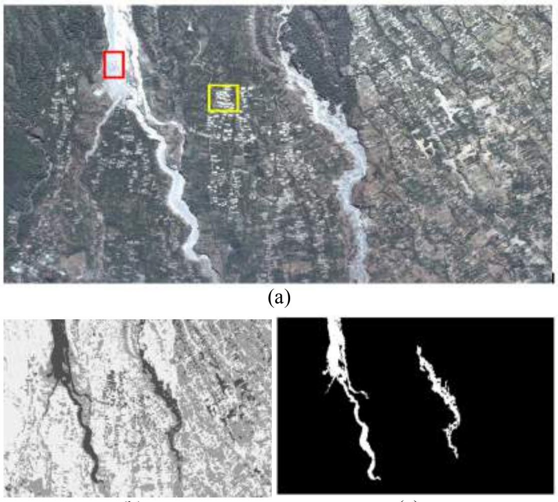

(a)

(b) (c)

Figure 7. Example of our land cover classification by color and size. (a) Example of sand river (red) and building (yellow), (b) Sand river and building are classified into, (c) sand river is separated by its size same class (labeled as black)

3.5.2 Impact Assessment and Impact in Number

After classifying the image set (Before, After, Now), we can perform several comparison between these images. We compare five comparison, as shown in Figure 2. Figure 2a shows the impacted area. We define impacted area as those pixels that change classes between Before and After, but not those that changes into vegetation (because it may happen naturally from open area to vegetation due to plant natural growth).

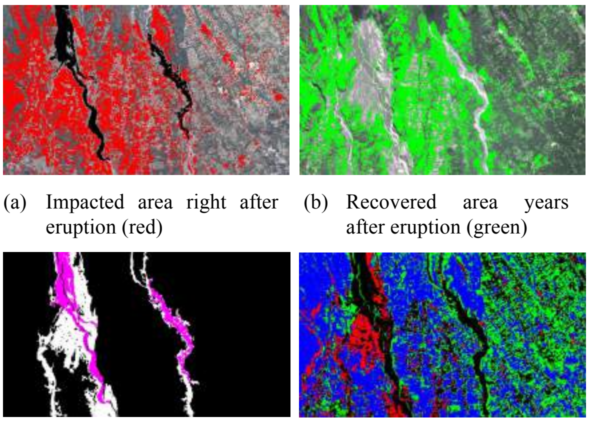

(a) Impacted area right after eruption (red)

(b) Recovered area years after eruption (green)

(c) Difference of river path before (magenta) and years after eruption (white)

(d) Difference of vegetation before and years after eruption

Figure 8. Impact Assessment

To quantify the number of impact and recovery area, we calculate two main impact caused by a volcano eruption such as a) the sand river expansion and b) number of building before the eruption and current situation. Table 1 shows how the sand river was expanded after the disaster and Table 2 shows the number of building before the eruption and the number of recovered building.

Table 4. Sand River expansion

Measurement	Value
Number of area after the eruption (in pixel)	4 times before eruption
Average width expansion after the eruption	4.5 times before the eruption
Maximum width expansion after the eruption	49 times before the eruption

Table 5. Number of Recovered Building

Time	Number of Building
Before the eruption	4281 building identified
Current condition (after recovery)	2568 building identified

4. CONCLUSION

As has been explained in the previous section, this research aims to detect and estimate the changes in the affected areas eruption of Mount Merapi in the time series. Through the study of the theoretical foundations and the analysis of results obtained with different techniques and methodologies that have been presented. The result makes it possible to develop algorithms to change detection on the surface due to the eruption of events. Furthermore, with different scenarios, methodologies have been applied may be contributing to the monitoring and investigating the possibility of an eruption event if deformation occurs in the volcano. Finally, through a process developed and various tests, the hypothesis were established at the beginning of this work can be considered and developed for similar studies.

5. REFERENCES

[1] Abrams, M., S. Hook and M. Abrams, (2002). "Imaging spectroscopy in the thermal infrared", Imaging Spectroscopy Applications. F. van der Meer and S. de Jong, Eds. Netherlands, Kluwer Academic Publishers.

[2] Abrams, M., Hook, S., dan Ramachandran, B. (2002). ASTER User Handbook: Version 2. Jet Propulsion Laboratory/California Institute of Technology.

[3] Chander, G. & Markham, B.L. (2003). Revised Landsat-5 TM radiometric calibration procedures, and post-calibration dynamic ranges. IEEE Transactions on Geoscience and Remote Sensing, 41, 2674-2677.

[4] Fernández L, Álvarez G, Salinas R. (2012) Impact area determination of pyroclastic deposits in Lascar volcano, eruptive process in the year 1993. Natural Hazards. Vol. 60 (2), 747–760. doi: 10.1007/s11069-011-0048-6

[5] Haralick R, Shanmugam K, Dinstein I. (1973). Textural features for image classification. IEEE transactions on Systems, Man, and Cybernetics. Vol. SMC-3 (6), 610-621. doi: 10.1109/TSMC.1973.4309314

[6] Jiménez-Escalona, J.C., Granados, H.D. & Realmuto, V.J., 2011. Use of MODIS images to study eruptive clouds from volcan de fuego de colima (Mexico) and applications on volcano monitoring. Geofisica Internacional, 50(2), pp.199–210.

[7] Joyce, K.E. et al., 2009. A review of the status of satellite remote sensing and image processing techniques for mapping natural hazards and disasters. Progress in Physical Geography, 33(2), pp.183–207.

[8] Kervyn, M., Kervyn, F., Goossens, R., Rowland, S. K., Ernst, G. G. J.(2007). Mapping volcanic terrain using high-resolution and 3D satellite remote sensing. Mapping Hazardous Terrain using Remote Sensing, Geological Society.

[9] Legeley-Padovani, A. et al., 1997. Mapping of lava flows through SPOT images an example of the Sabancaya volcano (Peru). International Journal of Remote Sensing, 18(15), pp.3111–3133.

[10] Ortiz R. 1996. Riesgo volcánico. Serie Casa de Los Volcanes N° 5. Servicio de publicaciones del Cabildo.

[11] Thome, K., P. Slater, K. Arai, S. Hook, H. Lang, F. Palluconi, H. Kieffer, T. Matsunaga, A. Ono and H. Sakuma. (1998). ASTER preflight and inflight calibration and the validation of Level 2 products. IEEE Transactions on Geoscience and Remote Sensing, 36(4): 1161-1172.

[12] Walter, T.R. et al., 2013. Volcanic eruption monitoring by thermal image correlation: Pixel offsets show episodic dome growth of the Colima volcano. Journal of Geophysical Research: Solid Earth, 118(4), pp.1408–1419.

[13] Wiart, P.A.M., Oppenheimer, C. & Francis, P., 2000. Eruptive history of Dubbi volcano, northeast Afar (Eritrea), revealed by optical and SAR image interpretation. International Journal of Remote Sensing, 21(5), pp.911–936.

Physical Vulnerability Modeling Based On Flood Inundation Model and Image Mining

Edy Irwansyah
Computer Science Department
Bina Nusantara University
Jakarta, Indonesia
edirwan@binus.ac.id

Guruh Samodra
Environmental Geography Department
Gajah Mada University
Yogyakarta, Indonesia
guruh.samodra@ugm.ac.id

Hendra Pachri
Geology Department
Hasanuddin University
Gowa, South Sulawesi, Indonesia
hendrapachri@unhas.ac.id

Maulana Ibrahim Rau
Civil and Environmental Engineering Department,
Bogor Agricultural University
Bogor, West Java, Indonesia
maulanaibrau@apps.ipb.ac.id

Muhammad Subair
Pulse Lab Jakarta
Jakarta, Indonesia
muhammad.subair@un.or.id

ABSTRACT

Flash flood disaster occurred within the City of Garut, West Java, Indonesia, on 20th September 2016, which caused many casualties and damages. Flood model could be performed to model the already-occurring disaster, as well as to depict future events that may occur to overcome any potential disasters, where the inundation flood model depicted the element at risk. In order to assist the analysis for the damages occurred, image mining could be used as part of the approach, where online media was utilized as well. The image mining resulted information about building damages caused by the flood. Afterwards, the physical vulnerability (buildings/residents) model could be further performed. Finally, the relationship between vulnerability and the flood inundation were portrayed. The resulted physical vulnerability model showed that larger height of the flood water caused higher degree of loss of the building, in which portrayed the need for total rebuild of houses as well. Considering available open source data and fast data acquisition, the approach showed such efficient approaches, where the results could be used in order to establish recommendation for building reinforcement, spatial planning, or protection wall in flood prone areas within the future time.

Keywords

Flash flood; flood inundation model; element at risk; building damage; image mining; physical vulnerability model

1. INTRODUCTION

Indonesia always has unique problematic matters in terms of water. Apart from drought that happens occasionally in Indonesia, flood always has its own attention in the country. Water-related problems not only result technical issues, but often impact the major economic and social perspectives of the nation. Having complex socio-economic problems, weak infrastructure and high population density, such conditions show that water-related disasters may cause more casualties in Indonesia. In Garut, West Java, Indonesia, on the 20th September 2016, flash flood occurred within the area, causing many impacts. Having the city to be around 24 kilometers from the east part of the forest that maintains the Cikamiri Water Spring, Garut lies within Cimanuk Watershed, in which has a total area of 3,636 km^2. The flood disaster caused death of 34 people, where 19 people gone missing. Also, 1,326 people was evacuated from the area, in which 2,511 residents were damaged (⅓ of them could not be utilized at all) [1]. It was said that the disaster was one of the worst disaster happening to the city.

Water is somewhat risky to the society if it is not handled properly, especially those related to flood. However, flood events are somehow predictable if they are well-calculated, where mitigation scenarios could be carried out beforehand, therefore, hydrological modeling is significantly important. Hydrological modeling is very pertinent in terms of disaster risk, since replicating natural systems may portray potential projected situations/impacts for the future time. Mentioned by Yoon *et al* (2014), to prevent water disasters, it is essential to develop management models that could support in settling upstream with downstream interests. Based on the disaster in Garut, the flood model could be performed as well, where further studies could be attained, including element at risks and the vulnerability of the residents/settlements surrounding the area of flood.

On the other hand, as part of the flood occurred in Garut, online media indeed had their own portion in informing the disaster. The media includes social media (such as Twitter, Instagram, etc) and many Indonesian electronic news. To overcome the problem in Garut, online media could be used as one of such approaches to depict the level of damages. Overcoming the condition in Garut, to depict the flood occurrence as well as to prevent any other disasters within the future time, the integration of both hydrological modeling and image mining (from online media) could be one of the most potential approaches. Hence, this study will be relevant for related stakeholders since it can assist decision making and cost–benefit analysis of structural protection measures by assessing the potential cost of future events, which can be used as well for other types of hazards within the future time.

[1] http://news.liputan6.com/read/2613863/journal-hutan-keramat-di-balik-banjir-bandang-garut

2. METHODOLOGY

Initially, the distribution of frequency was statistically identified to obtain the recurrence interval or return period, where the geomorphological condition of the catchment area was also carried out. Afterwards, as soon as all hydrological parameters were attained, flood inundation modeling could be performed. The result of the flood model were then used to show the element at risk, where potential building damages were observed, based on the integration of both risk and actual damages caused, derived from image mining, available via online media. Finally, the correlation between the resulted damages and resulted model could be depicted. The resulted model includes both velocity and depth value of the flood inundation.

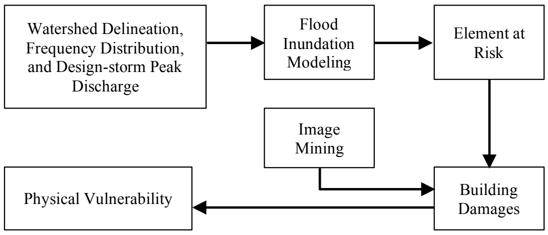

Figure 1. Methodology flow chart

2.1 Watershed Delineation, Frequency Distribution, and Design-storm Peak Discharge

The watershed delineation work was done based on the topography data provided by The Indonesian Geospatial Agency (*Badan Informasi Geospasial*), with contour data of 1:25,000. On the other hand, the rainfall data was derived from Garut's local Indonesian Agency for Meteorological, Climatological and Geophysics (*Badan Meteorologi, Klimatologi, dan Geofisika*). The rainfall data used for this study was 10 years, starting from 2002 to 2011. The frequency distribution was statistically calculated as well using the Gumbel Method (Al-Mashidani *et al*, 1978), to gain the peak designed precipitation. Afterwards, the design-storm peak discharge was further calculated using the rational equation (Kuichling, 1889). The values was then ready to be inputted to further perform the flood inundation model.

2.2 Flood Inundation Modeling

Flood inundation modeling was done using Hydrologic Engineering Center – River Analysis System (HEC-RAS) software developed by the U.S. Army Corps of Engineers (USACE). As part of the modeling process, the determination of geometric parameters for the system was carried out using HEC-GeoRAS software. The software enables users to perform the geometry of the specified stream based on its original topography. Within the process, parameters such as cross sections, channel banks, stream lines, as well as hydraulic parameters were calculated and were ready to be imported to HEC-RAS. Afterwards, in HEC-RAS, all related hydrological data (100-year return period) was then inputted to perform flow analysis, in which resulted the flood model inundation.

2.3 Image Mining

Internet, especially website and social media such as Facebook, Instagram and Twitter has accumulated a huge number of images contributed by their users. Filtering and downloading images automatically from internet using Application Programming Interface (API) from each of these social media and Google images or custom search API are available. Furthermore, with regard to disaster (demonstrating the impact of disaster), the images that can be used in this research must have two mandatory information, i.e. time and geolocation.

Mostly all images provided the time information in metadata or otherwise automatically or manually extract the time information from the posting time, caption of the images or from the text of articles are available. Whist for geolocation, a large portion of images uploaded to internet contain no geolocation information. Basically, the geolocations of images or photos in internet come from two sources: 1) With GPS-enabled cameras or gadgets, geolocations can be automatically extracted from the images or associated with the post in social media; 2) Users can also manually geotag photos by dragging a photo to a point on a world map interface or specific location name when uploading photos to an image sharing service or social media (Bo *et al*, 2014).

2.4 Element at Risk

An essential part in methodologies for the assessment of hazard - risks and vulnerabilities of physical and social structures is the identification and valuation of an inventory of objects and assets exposed to a certain hazard. The risk of an asset or element at risk is then expressed in its tendency to get damaged (Douglas, 2007). In the framework of the International Strategy for Disaster Reduction (ISDR) the term risk is defined as the "probability of harmful consequences, or expected losses (deaths, injuries, property, livelihoods, economic activity disrupted or environmental damage) resulting from interactions between natural or human - induced hazards and vulnerable conditions" (ISDR, 2004).

Consequently, risk assessment is based on a methodology to evaluate the nature and extent of risk determined by characteristics of potential hazards and conditions of vulnerability that could potentially harm people, their properties and the environment (ISDR, 2004).

In the evaluation of the risk that a certain element might be affected by a natural hazard, the exposure of the element has to be evaluated. The term exposure "refers in general to the volume and concentration of elements in a given area, and is calculated combining population exposure, density of population, built area, industrial area, and Government and institutional area" (Villagrán de León, 2006).

Thereby the distribution and characteristics of elements at risk can define physical exposure to natural hazards, e.g the susceptibility to be affected by natural phenomena: "Elements at risk, an inventory of those people or artefacts that are exposed to a hazard".

2.5 Building Damages

The main focus in this study is about the damage to the building units as an impact of flash flood. Damage to the building is recognized based on the information of the physical condition of each unit derived from photo images of buildings of various social media such as Facebook, Instagram and Twitter in the period of time of the incident and after the occurrence of Garut flash flood. The level of building's damage was based on physical criteria damage to buildings published by the Bakornas PB (Bakornas in Dept. PU, 2006) and was specially modified for flood damage in 2012 (Rijal, 2012).

2.6 Physical Vulnerability

Physical vulnerability is the potential damage defined by physical structure (material and construction building) when disaster occurred (Ebert *et al*, 2009). It can also be defined as the degree of loss to an element at risk (UNDRO, 1984). The vulnerability assessment is important for the development of disaster risk reduction strategies. Vulnerability is usually expressed as the value from 0 to 1 expressing the degree of loss due to the impact of the process. The relationship between vulnerability and the process of disaster is often described with vulnerability curve. The curve could be a valuable tool for the local authorities because it can assist decision making and cost–benefit analysis of structural protection measures by assessing the potential cost of future events. This can also be used for other types of hazards in the future. The vulnerability curve represents the function of the intensity of the process and the degree of loss.

3. RESULTS AND DISCUSSIONS

3.1 Watershed Delineation, Frequency Distribution, and Design-storm Peak Discharge

Prior undertaking all related flood modeling work, the geomorphological feature of the watershed/catchment area was required to be attained by delineating the watershed based on a specified downstream point. The delineation of catchment area is needed since the area will be specified to those areas that affected the downstream area only.

Figure 2. Catchment area with Copong Dam as downstream

The delineation was based on elevation data (1:25,000 scale) provided by the Indonesian Geospatial Agency (*Badan Informasi Geospasial*). The contour data was converted to Digital Elevation Model (DEM), and was used as the base for the delineation. For this study, the downstream point was Copong Dam, located at 821606 mE and 9204322 mN. Since the outlet of the catchment area was Copong Dam, the catchment area that potentially affected the downstream was 471.32 km^2.

Precipitation data was attained from local measurements, provided by Garut's local Indonesian Agency for Meteorological, Climatological and Geophysics (*Badan Meteorologi, Klimatologi, dan Geofisika*). The rainfall data used for the analysis was 10 years, starting from 2002 to 2011. From such data, as for the frequency distribution, the Gumbel Method was used for the analysis. With 100 return year period, the design rainfall was 228.03 mm. From the aforementioned design precipitation, the maximum design-storm peak discharge was then calculated as well, i.e. 304.14 m3/s.

3.2 Flood Inundation Modeling

Based on hydrological parameters gained, the flood model could be performed. The establishment of the model used Hydrologic Engineering Center – River Analysis System (HEC-RAS). The determination of the geometric parameters were based on the DEM data carried out previously, assisted by HEC-GeoRAS software. As for this analysis, 100-year flood return period (1% annual probability) was chosen.

From the analysis, the distribution depiction for the flood inundation was achieved. Based on the model, as results, both depth and velocity of the flood model was attained as well.

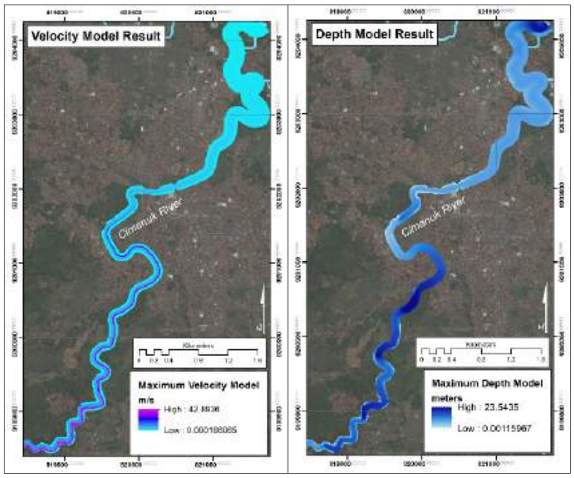

Figure 3. Flood inundation model results - velocity model (left) and depth model (right))

3.3 Image Mining

With regard to image mining, in most cases, the number of disaster related images that have valid time and geolocation will be very small and not representative, therefore manually finding and giving geolocation for images related with the disaster is necessary. However, giving geolocation for images manually can be very difficult and error prone, especially if users are not really familiar with the location and only have little information pra and post disaster. The workaround for this issue is only looking for special landmarks or points of interests which are easily recognizable and unambiguous, such as school, hospital, mosque, government offices, etc. The steps can be began by finding the specific landmark around the disaster site, obtaining the geolocation, and afterwards finding the landmark images, or vice versa starting with a list of existing landmark images. The point location for each area was then inputted to GIS. The results for the image mining were the determination of 43 buildings surrounding the area of flood to be indicated as damaged (Figure 4), which is further described on Section 3.4 and 3.5.

3.4 Element at Risk

Based on the previously described methodology, a case-study for flood prone areas of the city of Garut was carried out to identify elements at flood risk of the category of essential facilities (residents/buildings).

The identified tags by image mining approach were then extracted from the database on a map as point-information to derive a spatial representation of the relevant objects. In the last step of our methodology, the extracted data can be intersected with hazard maps to derive an indication about the exposure of the identified elements at risk. This approach of identifying elements at risk could be equal for every hazard.

Based on image mining approach, in the HEC-RAS model, corresponding to the essential facilities, the database of facilities for the city boundary of Garut was identified. Our study results showed that 43 buildings were damaged with the flash flood in the City of Garut (Figure 4). The intersection with a flood-hazard map for Garut resulted a list of five classes of the category of "element risk" exposed to flood-hazard (Table 1).

Figure 4. Element at risk depiction of essential facilities (residents/buildings)

3.5 Building Damages

Criteria of building damages as a result of flash flood for each level of damage can be seen in Table 1.

Table 1. Physical criteria to identify level of the building damage casused by flood

No	Level of Damage	Damage Criteria
1	Collapsed	Buildings are collapsed by flooding, where the overall building is buried by flood or most structures are damaged (inundated >50 cm and > 50 % part of building collapsed)
2	Severely Damaged	The building is still complete, but most of the structural components and architectural components are damaged (inundated max 50 cm)
3	Moderately Damaged	The building is still complete, but small part of the structural components and architectural components are damaged (inundated > 30 cm)
4	Slightly Damaged	The building is still complete, but no structural components are damage and only architectural components are damaged (inundated < 30 cm)
5	Non Damaged	The building is still complete, but no structural components are damage only inundated by flood (inundated < 20 cm)

Based on physical criteria on Tables 1, images of each building identified the extent of the damages. The main problems encountered was that most of the images were not complemented by location identifiers (coordinates) so that the identification of the building was only done to the building which was the city landmarks such as hospitals, schools and government offices. City landmarks were easily recognizable to obtain the identity of its location. The results of the identification of Garut city landmark building damage is seen in Table 1 and Figure 5.

Figure 5. Images and level of damage classification

Using coordinate information, each level of building damage can be mapped to see the distribution of the damage. Overlay distribution of damage map and the expansion of the inundation can be analyzed, showing the spatial impact of the flood occurring to the building (Figure 6).

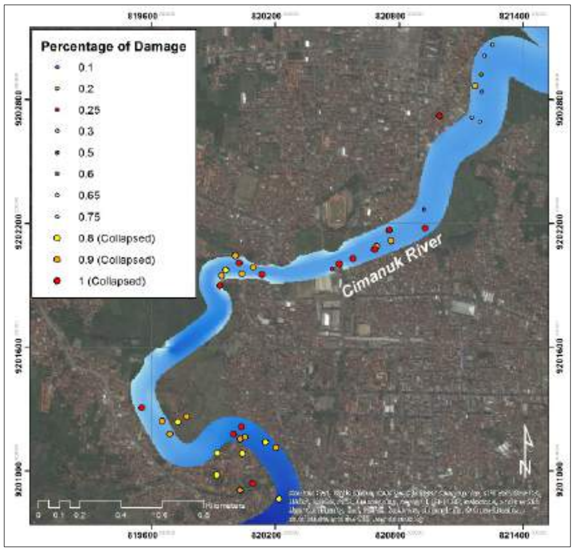

Figure 6. Spatial depiction of the damaged residents

3.6 Physical Vulnerability

The intensity of the Garut Flash Flood had been done on the basis of the flood height and flood velocity. The degree of loss was evaluated based on the damage assessment as the impact of flash flood. The photographic documentation obtained from image mining technique was used in order to assess the damage of the building. Following the assessment of flood intensity, the pictures showing the damage of each building were analyzed. The relation between the intensity of the flood and the degree of loss for each building is plotted in a two dimensional chart (Figure 7 and 8). The vulnerability curve shows that the larger the height of the flood water, the higher the degree of loss of the building. The curve becomes significantly steeper after the intensity of 6 m. The degree can also show the need for total rebuild of houses. The needs for total rebuild of houses starts with the intensities of 6 m.

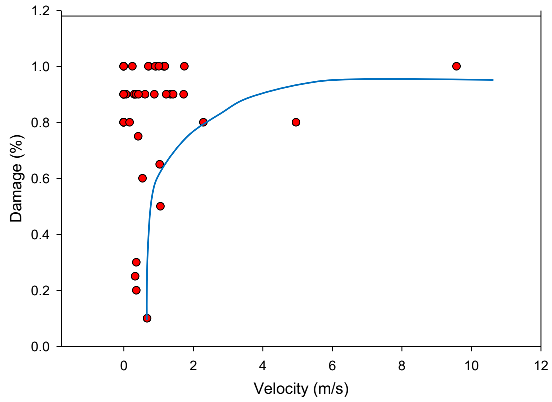

Figure 7. Correlation between damage and velocity

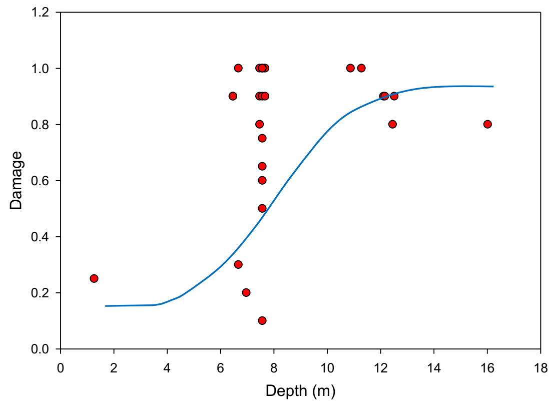

Figure 8. Correlation between damage and depth

The developed vulnerability curve can be applied in the risk assessment regarding flash flood events. The information derived from vulnerability curve is important for risk management. It could be used in order to make recommendation for building reinforcement, spatial planning, or protection wall in flood prone areas. Possible recommendations for specific objects to reduce their vulnerability could include keeping the distance from the river. The end users can employ the curve not only to calculate the costs of a future damaging event of a specific intensity but also to calculate the costs of an event if the position of the building changes. The cost-effectiveness of measures strategy including protection measures can also be analyzed by using the vulnerability curve. Protection measures such as wall can change the intensity of the flood on specific building. For example, the intensity of the flood on the specific building will be reduced by introducing a protection wall in a segment of river bank.

4. CONCLUSION

Considering available open source data and fast data acquisition, the study showed that that inundation model and image mining is one of such efficient approaches to depict the correlation between damage level of physical features (buildings/residents) and the flood inundation (velocity and depth) of the already-occurring flood disaster and potential future events. The resulted physical vulnerability model showed that larger height of the flood water caused higher degree of loss of the building, where it portrayed the need for total rebuild of houses as well. The results could be used in order to make recommendations for building reinforcement, spatial planning, or protection wall in flood prone areas within the future time.

5. ACKNOWLEDGMENTS

Huge gratitude for Pulse Lab Jakarta for providing all necessary technical and non-technical goods for this study.

6. REFERENCES

Al-Mashidani, G., Pande, B. B., Mujda, M. F. (1978) A simple version of Gumbel's method for flood estimation / Version simplifiée de la méthode de Gumbel pour l'estimation des crues, Hydrological Sciences Bulletin, 23:3, 373-380.

Bo, L., Quan, Y., Gao, C., and Dong, X. (2014) Where your photo is taken: Geolocation Prediction for Social Images. Journal of the American Society for Information Science and Technology (JASIST), Volume 65 Issue 6, pages 1232-1243, June 2014.

Departemen Pekerjaan Umum. (2006) Program Rehabilitasi Gempa D.I. Yogyakarta dan Jawa Tengah. http://ciptakarya.pu.go.id/dok/gempa/main.htm. Accessed on 17 March 2016.

Douglas, J. (2007) Physical Vulnerability Modelling in Natural Hazard Risk Assessment,Natural Hazards and Earth System Sciences , 7, 283–288.

Ebert, A., Kerle, N., and Stein, A. (2008) Urban Social Vulnerability Assessment with Physical Proxies and Spatial Metrics derived from Air- and Spaceborne Imagery and GIS Data. Nat Hazards 48:275-294.

ISDR (2004) Living with Risk: A global review of disaster reduction initiatives. International Strategy for Disaster Reduction. Switzerland: United Nations.

Kuichling, E. (1889). The relation between the rainfall and the discharge of sewers in populous districts. Transactions, American Society of Civil Engineers 20, 1–56.

Rijal, S. S. (2012) Analisis Kerusakan Permukiman Akibat Banjir Lahar Pasca Erupsi Gunungapi Merapi 2010 Di Sebagian Kabupaten Magelang (in Bahasa). Un-Publised Thesis.

UNDRO (1984) Disaster prevention and mitigation-a compendium of current knowledge. Preparedness aspects, vol 11, New York

Villagrán de León, J. C. (2006b) Vulnerability. A Conceptual and Methodological Review Studies of the University: Research, Counsel, Education -Publication Series of UNI-EHS, 4, Bonn, Germany

Yoon, T., Rhodes, C., Shah, F. A. (2015) Upstream water resource management to address downstream pollution concerns: A policy framework with application to the Nakdong River basin in South Korea, Water Resour. Res., 51, 787–805

Pulse Lab Jakarta is grateful for the generous support from
the Department of Foreign Affairs and Trade of the Government of Australia.